# Capturing 3D Continuum Effects in a 1D Soil-Structure Interaction Model for Seismic Analysis of Offshore Wind Turbines

R.P. Verlinde

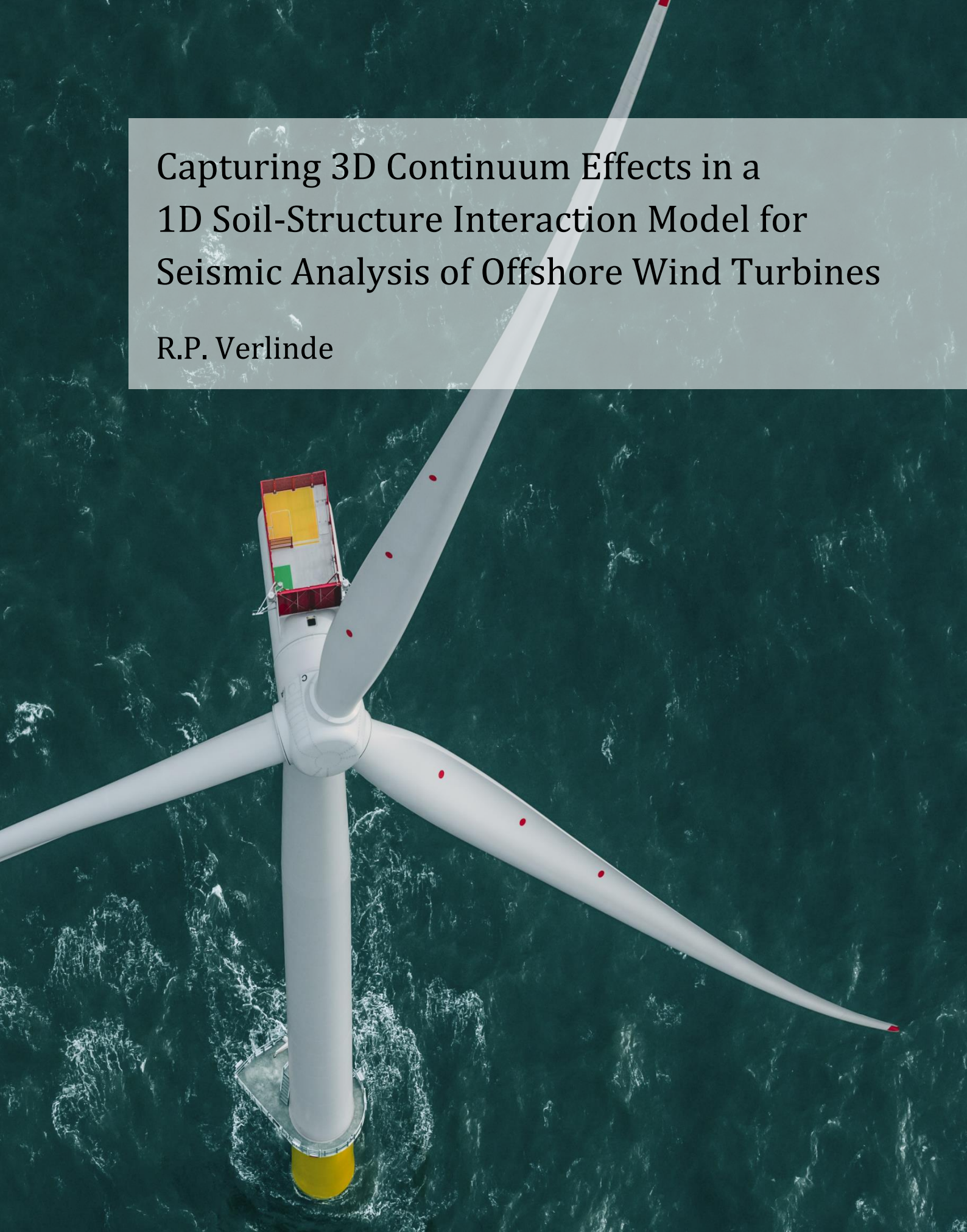

TU Delft

SIEMENS Gamesa
RENEWABLE ENERGY

# Capturing 3D Continuum Effects in a 1D Soil-Structure Interaction Model for Seismic Analysis of Offshore Wind Turbines

by

R.P. Verlinde

to obtain the degree of Master of Science
at the Delft University of Technology.

| | | |
|---|---|---|
| Student number: | 4251547 | |
| Project duration: | September 2018 - July 2019 | |
| Thesis committee: | Prof. dr. ir. A.V. Metrikine, | TU Delft - Chairman |
| | Dr. ir. K.N. van Dalen, | TU Delft |
| | Dr. ir. A. Tsouvalas, | TU Delft |
| | Ir. W. van der Linde, | Siemens Gamesa Renewable Energy |
| | Dr. ir. W.G. Versteijlen, | Siemens Gamesa Renewable Energy |

# Contents

# Summary

Offshore wind energy is considered a necessary energy resource, that may stimulate the transition from fossil fuels. Following the successful development in Western Europe, offshore wind is quickly gaining momentum in the Asia-Pacific region. At variance with North-Sea based offshore wind turbines (OWTs), structures installed in the Asia-Pacific region are exposed to a high risk of strong earthquakes. To reasonably manage these risks a solid understanding of the physical process of seismic loading is required. Moreover, accurate and effective design procedures to account for this complicated type of loading, need to be developed.

Considering that the response of OWTs to earthquakes is affected by the the interaction with the soil, the current thesis is aimed at providing a modelling method to accurately account for the effects of soil-structure interaction in the seismic design of offshore wind turbines. More specifically, the complicated load transferring mechanisms between the soil continuum and the most often applied monopile foundation are addressed. The accuracy of the currently applied design methods is questioned. The uncoupled lateral springs as used in these methods cannot capture the non-local reaction of the soil towards the rigid monopile. Moreover, these methods do not account for the effects of seismic wave diffraction as they use free-field ground motion to introduce the seismic action. For these reasons, the currently applied methods may provide inaccurate estimations of the seismic loads. Hence, more accurate modelling approaches are required.

In establishing the modelling method, it is suggested to benefit from the accuracy of a 3D model as it automatically captures the complicated 3D soil-structure interaction mechanisms during earthquake loading. For this reason, a 3D finite element model is provided that simulates the seismic loading of a monopile-supported wind turbine. The 3D modelling approach is however computationally too expensive to replace the simple, 1D models used in the design of offshore wind turbine structures. Therefore, to combine the speed and simplicity of a 1D model with the accuracy of the 3D model, the current thesis presents a method to obtain a 1D effective model that mimics the 3D modelled response.

In establishing the effective modelling approach, the 3D model is not only used as a target solution. The 3D model is directly employed to capture the 3D soil continuum reaction and the seismic excitation loads acting on the monopile. These components are incorporated into an effective model by making use of the substructuring method of analysis. To extract the 3D reactions of the soil, the non-local method of Versteijlen [30] is used. The soil stiffness matrices obtained by this method are integrated into a 1D beam model. The ground motion required to introduce the seismic action into this 1D model is determined in a separate step; the ground response analysis. This analysis is performed using a 3D model of the soil subsystem, that incorporates an excavation at the location of the embedded pile. This cavity is included to account for the effects of wave diffraction.

To assess, the performance of the provided modelling approach, a comparative study is performed between the 3D soil-structure model and the 1D effective model. This study showed that the 1D pile response closely matches the response of the 3D model - for both horizontal and vertical earthquake motion. Hence, it is proven that the developed design method effectively combines the accuracy of a 3D model with the simplicity of a 1D model.

Furthermore, the effective modelling approach is applied to assess the influence of 3D continuum soil-structure interaction effects on the structural response to earthquakes. These analyses indicate that the diffracted component of the seismic wave field does not significantly affect the earthquake excitation load acting on the monopile. As a results, the seismic wave diffraction can safely be neglected. This makes it possible to use free-field ground motion to introduce the seismic action into the effective 1D model. Moreover, the frequency dependent characteristics of the soil are evaluated - which are associated with geometric damping and inertial effects. An initial study on the influence of this soil frequency dependence, showed that the geometric damping results in a considerably reduced structural response for high frequencies. The effect of the soil inertia forces on the response to earthquakes is limited.

# Preface

This thesis is written as the final work to complete the Master's programme Structural Engineering with the specialisation Structural Mechanics at Delft University of Technology. The master thesis work was carried out in the collaboration with Siemens Gamesa Renewable Energy (SGRE) in The Hague. The topic was proposed by SGRE and further defined in collaboration with the TU Delft.

I was not able to perform and complete the research without the help of others. First and foremost, I would like to express my sincere gratitude to my graduation committee. From the TU Delft I want to thank Andrei Metrikine, Karel van Dalen and Apostolos Tsouvalas. Andrei, thank you for introducing me to the interesting field of structural dynamics and your useful comments when I needed to find the right focus. Karel, thank you for all the productive meetings. Your enthusiasm and positive feedback made it a pleasure to work with you. Apostolos, thanks for helping me to define the right scope within this interesting topic of seismic soil-structure interaction.

Special thanks to my daily supervisors at Siemens Gamesa Renewable Energy, Wouter van der Linde and Pim Versteijlen. Both your guidance really was invaluable to this work. Wouter, thanks for helping me to organize my thoughts during our fun weekly meetings. Your enthusiasm and support made it a pleasure to perform my thesis at SGRE. Pim, even though it was not even you that advised me to use the "non-local method of Versteijlen", I want to thank you for providing me with the knowledge and models required to perform this research. Moreover, your critical thinking and suggestions really helped me to keep the right focus throughout this project.

In addition to the committee members, thanks are given to Corine de Winter and Joao Barbosa. Corine, thanks for taking the time to discuss my work and guiding me in formulating the scope of my research. Joao, your input regarding numerical modelling helped me a lot in establishing the 3D and 1D models. Thanks a lot for the advice.

Furthermore, I would like to thank the SGRE team as a whole. The fun and academic atmosphere at the office in the Hague made my thesis experience so much more enjoyable. In particular, I would like to thank Adriaan, Landry, Friso, Sara and Tobias, for all the interesting discussions about the thesis work. But most of all, of course, thanks for the fun fussball games, vrijmibo's and coffee breaks.

Then of course, I want to thank Tessa for all the support and advice during the last few months. And lastly, thanks to all my friends and family members who have supported me during this thesis project.

*R.P. Verlinde*
*Delft, July 2019*

# 1 Introduction

In recent years, the offshore wind industry has experienced a huge growth. Although this industry is still primarily concentrated in Northwestern Europe, also other parts of the world start to benefit from offshore wind power as a mean of energy production. The environmental conditions at these locations provide new challenges as many of the areas are well known for their high risk of strong earthquakes. The impact of earthquakes on the structural integrity and stability of offshore wind turbines has only recently become of interest and is therefore a relatively new field of research.

With the recent development of offshore wind farms in seismically active areas comes the demand for better understanding of the requirements earthquakes impose on the design of substructures for offshore wind. Moreover, the development of adequate design and modelling procedures is required to accurately assess the seismic performance of offshore wind turbines. One subject that makes the earthquake analysis and design particularly challenging is the soil-structure interaction. The complexity of the soil-structure interaction during an earthquake results in many uncertainties in the design of a offshore wind turbine support structures. The guidelines used in offshore and earthquake engineering do not provide a structured framework on how to deal with these uncertainties, leading to the use of various design methods instead of a clear unified approach. Moreover, most design methods are established for (offshore) structures in general and are not developed for the large diameter tubular sections that characterize the monopile foundations. For this reason, more research into the structural behaviour of offshore wind turbine support structures and soil-structure interaction during earthquakes is required.

To provide further background on the topic of this thesis Section 1.1 will present an introduction to the earthquake analysis of offshore wind turbines. This is followed by a section specifically addressing the challenging field of seismic soil-structure interaction (Section 1.2) and finally, the objective of this thesis is established in Section 1.3 and an outline is presented in Section 1.4.

## 1.1. Earthquake analysis of offshore wind turbines

Research on offshore wind turbine structures has been mostly focused on the normal environmental conditions while, so far, relatively little attention has been spent on considering extreme natural hazards that threat the reliability of the wind turbines. Recently, studies have however indicated that loads induced by earthquakes may govern the design of offshore wind turbine support structures in regions with high seismicity (e.g. [1, 24, 28]), which highlights the importance of understanding the potential vulnerability of these structures during seismic events. Code provisions and technical guidelines also recognize the importance of earthquake-resistant design of offshore wind turbine structures and include brief recommendations on the seismic assessment procedures. Based on these guidelines and published research, the key aspects of seismic analysis of offshore wind turbines are discussed in this section.

As a wind turbine is a tall and slender structural system with a large mass at the top, it can be particularly sensitive to lateral forces and deformations, as induced by earthquake ground motion [36]. However, the relatively large flexibility of the conventional offshore wind turbine structures makes them insensitive to a

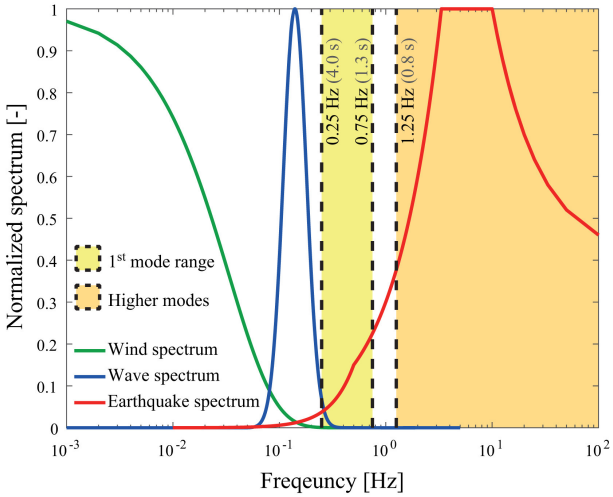


Figure 1.1: Frequency diagram showing typical normalized wind, sea wave and earthquake spectra along with the frequency ranges corresponding to first and higher vibration modes of conventional wind turbine structures (source: [6]).

great part of earthquake excitation frequency range [9]. This is visualized in Figure 1.1 by presenting a typical earthquake spectrum alongside with the frequency range corresponding to the first bending mode of conventional wind turbine structures. Nonetheless, numerous studies indicated that offshore wind turbines are not resistant against all seismic hazards. For specific earthquake characteristics, the seismic energy around the fundamental natural frequency may still be significant. Moreover, research has indicated that also higher modes of the structure may be significantly excited during a possible earthquake event [12]. Besides analyzing the seismic performance of the wind turbine's support structure, also the turbine blades need to be assessed [19]. As the resonant frequencies of the blades ($0.7-2.0$ Hz) correspond to the range of high seismic intensity, these components may be particularly vulnerable to earthquake action [10].

The seismic loads in earthquake analysis of OWTs are generally quantified by a time-history representation of earthquake excitations, which form the input for the method of response history analysis. This time domain method of analysis is preferred over frequency domain approaches for the analysis of OWTs, as it allows for adequate modeling of the complex aeroelastic interaction among the different wind turbine components [34]. The time-dependent operation of both the controller and the safety system can be efficiently modeled within the time domain, and thus, for example, the shutdown triggered by specified nacelle acceleration can be adequately analyzed [14]. The importance of considering a possible emergency shutdown in the seismic load simulations of OWTs is recognized by the design guidelines [22, 29]. Besides the emergency shutdown, two other operating scenarios should be accounted for according to these codes; normal operational conditions (running) and parked conditions (idling) [7].

The standards require the earthquake analysis in two horizontal directions as well as in the vertical direction. Numerous studies (e.g. [11, 17, 18]) recognize the potential vulnerability of offshore wind turbine structures to vertical seismic excitations. These indicated a strong amplification of vertical seismic motion that could possible cause structural failure of offshore wind turbines.

## 1.2. Seismic soil-structure interaction

The interaction between soil and structure has been found to be a critical aspect in the analysis and design of offshore wind turbines as it has a significant impact on the response of the structure to dynamic loading. At the same time, the highest modelling uncertainty in the design of offshore wind turbine foundations is related to this soil-structure interaction [26]. The soil reaction towards the rigidly behaving monopile (MP) is particularly challenging to describe as it conveys complicated soil-structure interaction (SSI) mechanisms that require advanced modelling techniques [30]. The knowledge gap in this field, most often results in conservative designs of the wind turbine support structures. However, due the many opposing effects in soil-structure interaction this can not always be guaranteed. Only through proper understanding of soil-structure interaction one can adequately consider (or conservatively neglect) SSI effects in engineering design.

Compared to the normal environmental loading conditions, accurate description of soil-structure interaction is even more important for earthquake loading of wind turbine structures. This is due to one fundamental difference; seismic loads do not originate from the structure towards the soil, but from the soil towards the structure. This specific characteristic result in an additional role of the foundation; besides bearing the structures vibrations and transferring them to the ground, the foundation also transmits the ground motion to the structure. Therefore, the description of SSI in earthquake analysis is crucial for the determination of the load itself and an incorrect soil modelling can significantly over- or underestimate the dynamic response of the structure due to the seismic action.

**Effects of soil-structure interaction**
The primary effects of soil-structure interaction to the seismic response of structures include effects specific for earthquake loading conditions and effects related to the general dynamic response of structures. In general, the most apparent effect of soil-structure interaction is the increased flexibility of the system [2]. This results in a decrease of the fundamental frequency to a value significantly below that applicable for the fixed-base situation. Due to the increased flexibility, the shape of the vibration modes will change as well. Another important effect of the soil to the dynamic response of structures is the increased amount of damping due to soil material damping and geometric damping. These additional damping mechanism introduced by the soil may lead to a strongly reduced response of the structure [16].

The interaction between soil and structure also effects the seismic loads itself. This can be explained by looking at the process of earthquake loading. Due to a sudden release of energy, seismic waves start to travel through the earths interior and will cause earthquake ground motion. In the absence of a structure this motion is referred to as the free-field ground motion. When a structure is present at the surface, the seismic waves will at some point reach the structure's foundation and at the interface energy is partly scattered away and partly transmitted. Due to the energy transmitted to the structure, it starts to vibrate and alters the soil motion around it. During this process the motion of the structure will differ from the free-field ground motion as the equilibrium that needs to be satisfied at the soil-structure interface is not the one of a stress-free surface. The seismic loading transmitted to the structure therefore depends on the interaction between the soil and structure.

Due to the many opposing effects of soil-structure interaction, it is difficult to decide whether neglecting SSI effects is in general conservative or not [2]. For example, the effect of an increased flexibility of the system depends very much on the frequency content of the input motion. Moreover, the structural deformations can be significantly increased due to the effects of the soil.

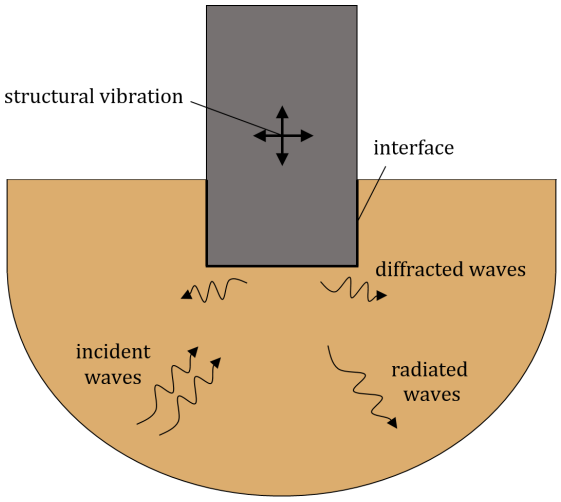


Figure 1.2: An impression of the soil-structure interaction process during seismic loading.

**Modelling methods for seismic soil-monopile interaction**
The commonly applied methods to incorporate soil-structure interaction effects in the seismic analysis of structures, can be separated in methods adopting a direct approach and modelling methods using the substructure method of analysis. In the direct approach the soil and structure are simultaneously accounted for in the mathematical model and analyzed in a single step. For a complex foundation-soil system, the direct analysis is often performed as time domain simulations using 3D finite element modelling. When adequately used, this approach accurately models the propagation of seismic waves through the soil and it is able to capture complex 3D interaction mechanisms between soil and structure. Moreover, since the assumptions of superposition are not required, true nonlinear analysis are possible. Nonetheless, the analyses are expensive in terms of computational time and require special consideration for modeling the fictitious boundaries of the soil domain to eliminate reflection of waves and to introduce the seismic excitation [2]. Hence, direct soil-structure interaction analysis are used only in special cases and are usually not applied for load simulations of offshore wind turbines [14].

In the design process of offshore wind turbines the response of the structure is of primary relevance and therefore an equivalent representation of the soil reaction with proper consideration of the seismic action usually suffices. To achieve this, the fully coupled system is often treated as two separate components by applying the substructuring method of analysis. In this approach, the responses of the soil and structure are first obtained independently and subsequently combined to formulate the complete solution. This is done by joining the soil and structure at the common interface by imposing force equilibrium conditions and kinematic compatibility at all times. As the substructure approach is based on superposition, this method is normally limited to linear behavior. The principal advantage of the substructuring approach is its flexibility. Because each step is independent of the others, it is easy to focus resources on the most important aspects of the problem.

An often-applied approach to account for the soil reaction in the analysis of offshore wind turbine structures is by making use of a Winkler type foundation [33]. This approach uses locally acting springs and dashpots along the embedded length of the monopile foundation to account for the impedance of the soil. In earthquake analysis of monopile-based OWTs the Beam-on-dynamic-Winkler-foundation (BDWF) model is employed by adopting the substructuring method of analysis. This commonly applied approach is based on two separate modelling stages. In the first stage, the free-field soil motions are computed using a suitable ground response modelling method. The second stage of the analysis computes the response of the structure supported by the Winkler springs. This is done by exciting the supports of these springs with the free-field soil displacement, while on at the other end the springs are connected to the pile. In this way, the seismic loads and displacements are introduced to the structure. This substructuring approach - as visualized in figure 1.3 - is relatively simple to apply in the seismic load simulations of OWT structures. Moreover, it provides a very intuitive visualization of the physical process of seismic soil-structure interaction as it directly yields a representation of the foundation response.

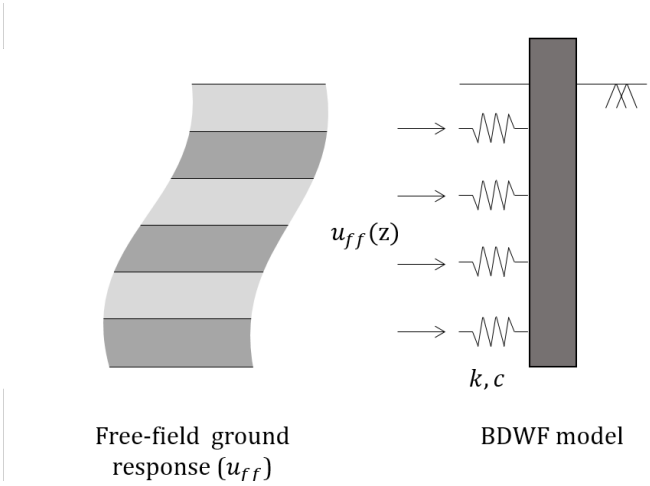


Figure 1.3: The conventional modelling procedure for seismic soil-pile interaction: the Beam-on-dynamic-Winkler-foundation model in combination with a free-field ground response analysis.

Even thought, the substructuring method of analysis based on the BDWF model in combination with free-field ground response analysis is well-accepted and has allowed the safe design of many structures, this approach does not fully capture the 3D seismic soil-structure interaction process of large-diameter monopile foundations. By assuming undisturbed soil conditions in determining the seismic ground motion, it is not accounted for that the presence of the structure alters the free-field seismic waves due to diffraction. While, the assumption of neglecting the diffraction can be substantiated for small diameter piles, this is not necessarily the case for the large monopile foundations. Therefore, adopting this approach results in additional modelling uncertainties in the seismic design process of offshore wind turbine support structures.

For determining the spring properties in the BDWF model, a great number of methods are available. The offshore wind industry adopted the $p-y$ curve approach [20, 23, 25]. This semi-empirical approach (established by the oil  gas industry) yields curves describing the local, nonlinear relation between soil reaction force ($p$) and pile displacement ($y$) at specific depths along the embedded pile. The Winkler spring stiffness is described by the tangent of these $p-y$ curves. However, as this method adopts uncoupled springs to represent the dominant soil reaction towards the rigidly behaving monopile foundations, the complete reaction of the soil is underestimated. The global restoring force of the soil is induced by more complex, non-local interaction mechanisms, which are not accurately captured by the $p-y$ curve approach. Therefore, adopting the nonlinear $p-y$ curve approach, further increases the modelling uncertainties in the seismic load simulations of wind turbines. The nonlinear spring stiffness representing the soil restoring force, is an empirical tuning parameter depending on the soil characteristics, the properties of the pile and the loading conditions. As the currently used $p-y$ curves were calibrated on small-diameter, flexible piles, under quasi static loads originating from the structure, these curves are not representative for the soil reaction during seismic loading of monopile foundations.

## 1.3. Objective

The development of offshore wind farms in seismically active areas presents support structure and wind turbine generator designers with the challenge of a new type of loading. Unlike other loads such as wind, waves and ice loads, seismic loads originate from the ground. The evaluation of seismic loading therefore not only requires understanding of the load transfer from the structure to the soil, but also from the soil to the structure. The interaction between soil and structure can considerably affect the dynamic response of offshore wind turbine structures. For this reason, modelling methods to simulate the response of offshore wind turbines to earthquakes are required, that do not only incorporate the structure but also account for the effects of soil-structure interaction.

The interaction between soil and monopile foundations during earthquake loading is a complicated 3D process where loads are transferred between soil and structure through different mechanisms. Hence, the seismic soil-structure interaction of these structures can best be captured by employing a continuum approach that considers the soil as a 3D solid. Currently, however, engineering models are applied that employ Winkler-type foundations in combination with free-field ground response analyses. The accuracy of this effective modelling approach for the seismic analysis of monopile-supported offshore wind turbines is questioned. First of all, the uncoupled lateral springs as used in the 1D Winkler model cannot capture the non-local response of the soil continuum towards rigid monopiles. Secondly, the use of free-field ground motion to introduce the earthquake action, does not account for the effects of seismic wave diffraction due to the presence of the structure. For these reasons, the currently applied 1D methods may inaccurately simulate the seismic response of offshore wind turbine structures to earthquakes.

Nonetheless, a 1D model is currently still required in the design process of offshore wind turbines as 3D models are computationally too expensive. Three-dimensional models can still be used for improved physical understanding of the soil-structure interaction during seismic loading of offshore wind turbines. However, to become truly useful for design, the 3D model should not only serve as a design check, but its accuracy should be directly integrated into the design models. For these reasons the objective of this thesis is:

**Establish a method to identify an effective 1D model for seismic analysis of monopile-based offshore wind turbines that incorporates 3D soil-structure interaction**.

Moreover, this effective method will be applied to assess the influence of 3D continuum soil-structure interaction effects on the offshore wind turbine's response to earthquakes. Based on this assessment, recommendations for the practical application of the effective modelling approach will be provided.

## 1.4. Outline

In order to meet the objectives of this thesis, several sequential steps are to be followed. This master thesis report is structured in accordance with these steps.

In Chapter 2, the required theoretical background on the physical process of earthquakes is provided in order to allow for an adequate representation of the seismic loading of offshore wind turbine structures. Next, in Chapter 3, a 3D finite element model is provided to simulate the three-dimensional interaction between monopile foundation and soil, yielding a more realistic estimation of the structural response to earthquakes than obtained with the conventional Winkler-type models. The modelled 3D response is used as a target solution for the effective modelling approach.

The method to identify the 1D effective soil-structure interaction model for seismic analysis of OWTs is presented in Chapter 4. The dynamic substructuring approach used for this purpose is introduced and the modelling steps to obtain the 1D model are presented. Subsequently, Chapter 5 provides the validation of the effective method by comparing the modelled 1D response with the response obtained with the 3D model. Moreover, the modelling limitations are discussed.

In Chapter 6, the effective modelling method is applied to assess the influence of 3D continuum soil-structure interaction effects on the response of offshore wind turbines to earthquakes. Based on this assessment, recommendations for the practical application of the effective modelling approach are presented. Finally, the main conclusions of the thesis and recommendations for extended research are given in Chapter 7.

# 2

# Theoretical background

In this chapter a literature study is performed with the objective of providing the theoretical background required to adequately model the seismic loading of monopile-based offshore wind turbines. In Section 2.1, the propagation of seismic waves is addressed and the different types of waves are introduced. In Section 2.2, focuses on the characteristics of earthquake induced ground motion. Finally, Section 2.3 discusses the local site effects and the ground response analysis.

## 2.1. Seismic wave propagation

An earthquake is manifested as ground shaking caused by a sudden release of energy in the earths crust. This energy may originate from different sources. Earthquakes induced by movement of tectonic plates are of primary relevance for the design and analysis of wind turbine structures [13]. These tectonic earthquakes originate due a relative movement of plates causing stress to build up at the interface. When the stress reaches a limit, a fault rupture occurs and seismic energy is released. This energy is converted into waves propagating away from the source. When reaching the surface of the earth, the waves will cause shaking of the ground.

Waves travelling through the earths interior are called body waves. When a wave approaches a surface, other types of waves can be formed. These waves are called surface waves as they travel along the surface instead of through a body. Body waves can be distinguished into two types; P-waves (primary/pressure) and S-waves (secondary/shear). The former are waves in which the particle motion is equal to the direction of propagation of the wave. Therefore, P-waves propagate by expansion and compression of the body they travel through. For S-waves the particle motion is perpendicular to the direction of wave propagation. At ground surface, S-waves can produce both vertical (SV) and horizontal (SH) motions. The velocity of a body wave depends on the stiffness and the density of the medium through which they pass. The velocity of P-wave in an isotropic and homogeneous solid can be calculated as:

$$v_p = \sqrt{\frac{G(2-2\nu)}{\rho(1-2\nu)}} \tag{2.1}$$

where $G$, $\nu$ and $\rho$ are the shear modulus, Poisson ratio and density of the medium, respectively. Since the rock and soil are rather resistant to the compression-dilation effects, the P-wave generally has a minor influence on the ground motion. However, especially at sites close to fault ruptures, P-wave may still generate significant ground excitation [13].

Compared to P-waves, shear waves generally cherishes a longer period with a lower wave speed ranging from 100 to 800 m/s for soils and around 3000 m/s for hard rocks. The velocity of S-wave in an isotropic and homogeneous solid is given by:

$$v_s = \sqrt{\frac{G}{\rho}} \tag{2.2}$$

Surface waves occur when (inclined) body waves interact with a surface, e.g. the surface of the Earth. Rayleigh waves and Love waves are the most relevant types of surface waves for earthquake engineering applications.

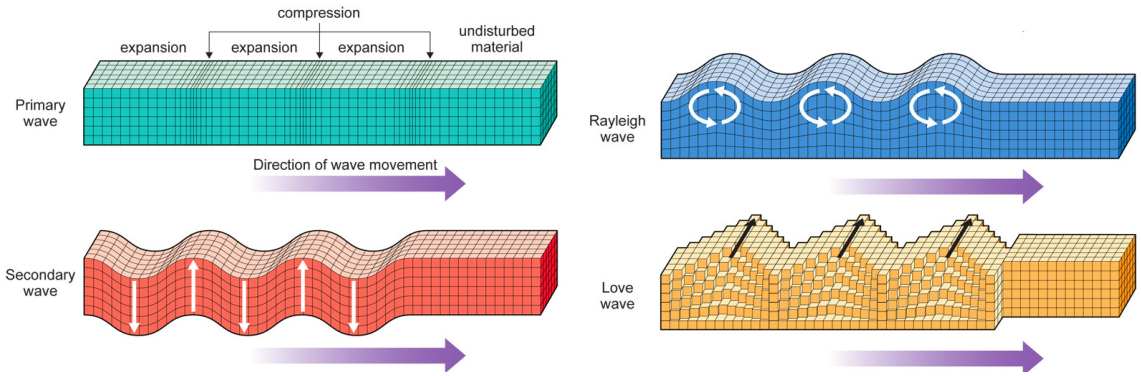


Figure 2.1: Motion caused by harmonic body and surfaces waves.

Rayleigh waves are produced by interaction of P- and SV-waves with the Earth's surface and involve both horizontal as vertical particle motions. Love waves are shear waves that are the result of SH-waves that interact with a soft superficial layer and have no vertical component of motion. Compared to body waves, surface waves have a longer period with a relatively slower decay with time.

The relative significance of body and surface wave forms depends on various factors such as source mechanism, source-to-site distance, direction to the source, topography and sediment geometry. Shear waves generally cause the ground motions that are most damaging for structures as the horizontal peak ground acceleration is mostly influenced by the S-waves, and only in some cases by surface waves. If the distance between the earthquake source and a site is larger than a few times the Earth crust thickness (30-50 km), instead of body wave, the surface wave is likely to produce the peak ground motions [13]. This is due to the surface wave's slower rate of decay than that of body waves. As a result of geometric spreading in 2D the energy carried by surface wave decays as $\frac{1}{R}$, with $R$ being the distance from the source. The energy carried by body waves decays with $\frac{1}{R^2}$, due to the spreading in three dimensions.

## 2.2. Earthquake ground motion

If a structure is build in a seismically active region and it is deemed to be affected by a potential earthquake, an estimation needs to be made of the possible ground motion induced by seismic waves. This is done by performing an assessment of the local seismicity, which accounts for the rupture mechanism at the source of the earthquake as well as the source-to-site attenuation characteristics. When the earthquake event is dominated by body waves, the procedure to determine the ground motion at the site of interest is generally divided into two parts. This is done by introducing an interface layer called the engineering bedrock; a relatively stiff layer underlying the soft soil deposit on which the structure is founded. The first step of the procedure is to identify the relevant motion characteristics (amplitude, frequency content and duration) of this bedrock layer, using probabilistic seismic hazard analysis (PSHA). The motion at bedrock is used as input for the second analysis step; the site response analysis. This site or ground response analysis captures the propagation of waves through the shallower soil layers to take local effects into account.

The composition of the seismic wave field at bedrock level is complex and depends on the regional geology and seismology. Due to (inclined) propagation of both P-waves and S-waves the motion of the bedrock is composed out of both horizontal and vertical motion components. For small epicentral distances ($\approx$ 20 km) the intensity of the vertical accelerations is roughly equal to that of the horizontal motions and falls off down to 50 to 30 percent for larger epicentral distances [32]. In practice, it is well accepted to derive the vertical bedrock motion spectrum by scaling the horizontal motion spectrum by either a constant factor or different factors at different frequency ranges [8]. Vertical motions are mainly caused by P-waves, and partially contributed to by SV-waves. Because the pressure wave velocities of the soil and the underlying rock generally have little differences, the motions at ground surface are essentially very similar, or can in many cases be assumed to be identical, to the vertical seismic motions at bedrock [13, 22]. Furthermore, seismic ground motions vary between different spatial locations. This spatial variation of the ground motions is attributed to source-rupture characteristics, wave propagation through the earth strata, scattering and local site effects.

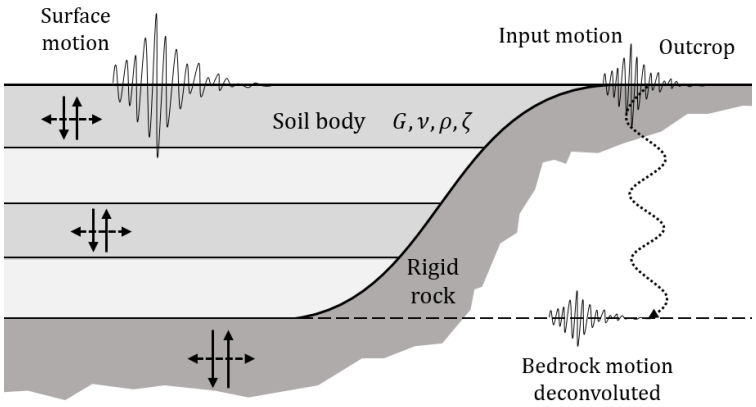


Figure 2.2: Visualization of the bedrock and ground surface motion.

For structures with small horizontal dimensions, it is usually reasonable to assume that the spatial variation does not significantly affect the structural response and therefore uniform motion along the bedrock can be assumed [27].

## 2.3. Ground response analysis

Whereas seismological considerations dictate the wave composition, amplitude, and frequency content of the incoming seismic motion in the underlying rock, the geometric and stiffness characteristics the soil deposit affect and modify (often profoundly) the ground motions experienced at the site. Reflections and refractions at the layer interfaces and the free surface, as well as resonance phenomena that may result from these, modify the wave field in the shallow layers with respect to the incident seismic wave field at bedrock. The motion of the soil deposit without the disturbance of an (embedded) structure or excavation, is referred to as the free-field ground motion. Based on the seismic input at bedrock level, this motion can be determined by performing a free-field ground response analysis.

Ideally, a full ground response analysis would model the rupture mechanism and evaluate how the waves propagate until reaching the site of interest. However, this mechanism is so complicated and unpredictable that such approach would not be practical. This is why different simplified 1D, 2D and 3D design methods for ground response analysis have been developed in order to approximate the ground motion based on the motion characteristics at bedrock level. Two-dimensional or three-dimensional methods may be required when irregular geometric properties of the site (such as sloping layer boundaries or basins) significantly affect the wave propagation or when different types of seismic wave propagation needs to be captured, i.e. body and surface wave.

For practical applications, generally one-dimensional analysis are adopted to determine the free-field ground response. One-dimensional analysis can be performed under the following assumptions:

- The boundaries between the different layers of the soil, the bedrock and the surface are horizontally stratified.
- The soil deposit and the bedrock extend to infinity in the horizontal direction.
- The motion of the bedrock is spatially uniform.
- The response of the soil deposit is predominantly caused by SH waves propagating vertically from the underlying bedrock.

The last assumption can be justified considering that seismic waves propagating from the source through the earths interior, are bent by successive refractions into a nearly vertical path (according to Snell's law of refraction).

Under the given assumptions, the motion of the soil column can be described by the following equation of motion:

$$\rho(z)\frac{\partial^2 u}{\partial t^2} = \frac{\partial}{\partial z}\left(G(z)\frac{\partial u}{\partial z}\right) + \frac{\partial}{\partial z}\left(c(z)\frac{\partial}{\partial t}\frac{\partial u}{\partial x}\right) \tag{2.3}$$

where $\rho$ is the density of the soil, $G$ the shear modulus and $c$ the damping coefficient.

Using this equation of motion, the free-field ground motion along the height of the soil stratum can be determined. Moreover, an estimation can be made of the resonance periods of the site. The site period $T_s$ for uniform single soil layer on bedrock can be estimated from the relationship:

$$T_{s,n} = \frac{1}{2n-1}\frac{4H}{v_s} \tag{2.4}$$

where $T_s$ is in seconds. $H$ and $v_s$ are the depth of the soil layer and soil shear wave velocity, respectively. $n$ is represents the $n$th mode of vibration ($n > 1$). For a complete derivation of the one-dimension shear wave propagation model, reference is made to [27].

# 3

# 3D soil-structure model

To capture the complex seismic wave propagation and soil-structure interaction mechanisms between MP foundations and soil during earthquakes, the pile must be modeled as embedded in a 3D continuum. In such a model the soil reaction and the seismic loads transmitted to the rigid monopile structure can accurately be identified. This direct approach models the soil and the structure in a single step and therefore requires fewer assumptions compared to the often applied Winkler-type modelling method, which is based on substructuring. Moreover, as both the soil and structure are explicitly modelled, the 3D modelling approach is not bound to the specific range of pile and soil properties for which they were tuned.

For simulating the seismic loading of offshore wind turbines on monopile foundations, a MATLAB based finite element model is used. The model is a variation on the model of Barbosa [15] and computes the response in the frequency domain. Originally the model was developed for loads acting at the top of the monopile. To suit the model for this work a superstructure is included and the model is modified to incorporate seismic loads originating from the soil. First, a description of the model is provided in section 3.1 and subsequently the numerical implementation will be discussed in section 3.2. In section 3.3 modelling results are presented and the response of the soil-structure system to earthquake excitation is discussed. Besides simulating the seismic excitation of the fully coupled soil-structure system, this model will also serve as a basis for the effective 1D modelling method. This will be discussed in Chapter 4.

## 3.1. Model description

A stratified soil deposit is considered in which a monopile foundation is embedded. On top of the foundation the superstructure is included, which consists of the tower and rotor nacelle assembly. The soil body overlays a rigid bedrock layer, on which the seismic load is introduced. A large dynamic impedance contrast is considered (e.g. low velocity sediments over high velocity bedrock), such that the bedrock layer can be modelled as a rigid boundary reflecting downward propagating waves back into the system. The seismic load acts in the global $x$ and $z$-direction and it varies in time harmonically. It is imposed as a dynamic displacement which is spatially-uniform over the full bedrock surface. In the horizontal direction, the outer boundaries of the soil domain satisfy the radiation condition such that the energy propagating away from the structure does not get reflected. The geometry of the model is presented in Figure 3.1.

### 3.1.1. Modelling of the structure

The monopile design used in this work is an idealized representation of a contemporary offshore wind turbine foundation. The MP is designed for a water depth of approximately 30 meter, has an embedded depth of 30 meter and a constant outer diameter of 7.0 meter. The pile thickness varies locally along the $z$-axis of the pile. For simplicity, this minor $z$-depency is omitted and the geometry of the foundation is assumed to be constant. The geometry of the tower is generally more complex and varies significantly over the height of the structure. However, as detailed modelling of this part is not required for the qualitative analysis of soil-monopile interaction, a simplified representation of this superstructure is employed; the tower is modelled with constant cross-sectional properties and the RNA is idealized as a lumped mass with rotational inertia. The idealized structural geometry as used in this work is presented in Table 3.2 - with reference to Figure

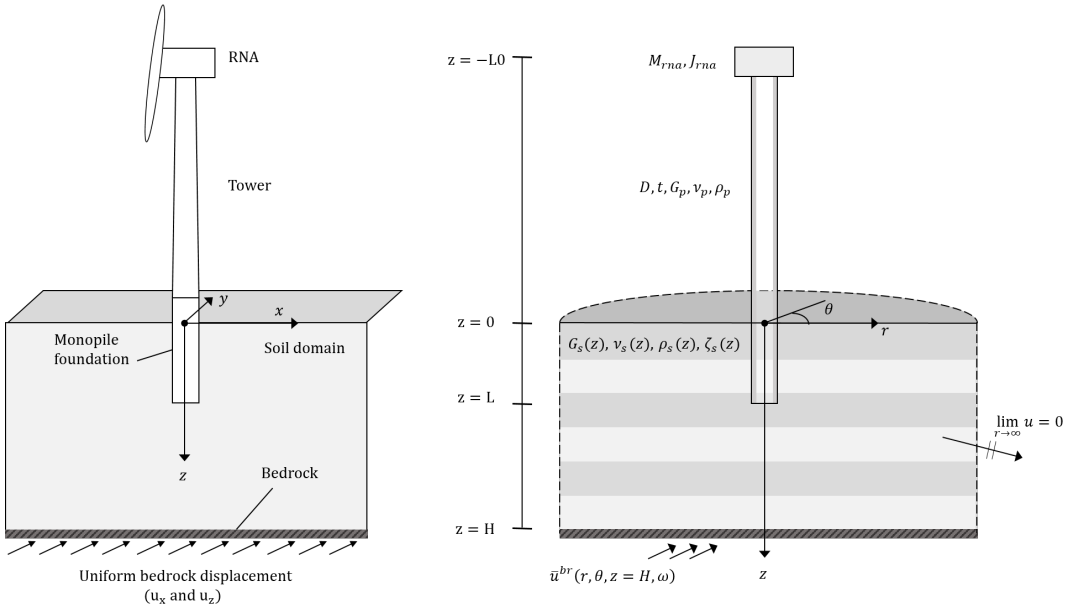


Figure 3.1: Geometry of the 3D soil-structure model.

3.2). These are determined such that the dynamic characteristics of the structure approach that of realistic offshore wind turbine structures. The material properties describing the linear elastic behaviour of the steel are also included in Table 3.2. These properties are modelled to be constant throughout the structure and no steel material damping is included.

### 3.1.2. Modelling of the soil body

Similar to the steel of the structure, the soil medium is modelled as an isotropic, linearly elastic solid. The material constants describing the behaviour of the soil vary along the depth and can be defined by the shear modulus $G_s$, poisson ratio $\nu_s$, mass density $\rho_s$. The material damping in the soil involves a frictional loss of energy. This so-called hysteretic damping is independent of frequency. It can be introduced into the equations by replacing the elastic constants by corresponding complex ones. In this model this is done by making the shear modulus of the soil $G_s$ complex:

$$G_s^* = G_s(1 + 2i\zeta_s sgn(\omega)) = G_s(1 + i\eta sgn(\omega)) \tag{3.1}$$

where, $\zeta_s$ is the damping ratio and $\eta$ is the loss factor. The complex continuum stiffness and the geometric damping cause the soil-structure response to become complex valued.

The soil profile used in this work is based on the Westermeerwind near-shore wind farm [30]. The characteristics as implemented in the model are presented in table 3.3. The variation of stiffness, Poisson's ratio, density and the corresponding shear wave velocity are presented in Figure 3.2. Besides the heterogeneous, realistic soil profile, a fictional idealized case with homogeneous properties is considered as well. The bottom soil layer, starting at a depth of 30 meters, is assumed to be extending up to the underlying bedrock. The is rigid bedrock layer is assumed to be located at a depth of 60 meter.

The soil profile is modelled to extent into the tubular pile section, such that monopile is filled with soil up to a certain level. In this work two limit cases are considered, one where there is no soil inside of monopile and one where the pile is filled with soil up to the seabed level. The last case is a more accurate representation of reality. However, due to soil plugging it may occur that part of the monopile is free of soil on the inside [4]. With these two different conditions and the two different soil profiles, a total number of four cases will be considered in this work. These are listed in table 3.1.

| Case | Soil profile | Soil inside monopile |
|---|---|---|
| 1A | Homogeneous | Yes |
| 1B | Homogeneous | No |
| 2A | Heterogeneous | Yes |
| 2B | Heterogeneous | No |

Table 3.1: Case studies considered in this work.

| Property | Symbol | Value | Unit |
|---|---|---|---|
| Pile tip - Mudline | $L$ | 30 | m |
| Mudline - Hub height | $L_0$ | 130 | m |
| Outer diameter | $D$ | 7.0 | m |
| Wall thickness | $t$ | 0.07 | m |
| RNA total mass | $M_{RNA}$ | $450 \times 10^3$ | kg |
| RNA rotational inertia | $J_{RNA}$ | $65 \times 10^6$ | kg m$^2$ |
| Youngs's modulus | $E_p$ | 210 | GPa |
| Poisson's ratio steel | $\nu_p$ | 0.3 | - |
| Density steel | $\rho_p$ | 7850 | kg/m$^3$ |

Table 3.2: Geometry and material properties of the structure.

| Property | Symbol | Value | Unit |
|---|---|---|---|
| Bedrock - Mudline | $H$ | 60 | m |
| Shear modulus soil | $G_s$ | Fig. X | MPa |
| Poisson's ratio soil | $\nu_s$ | Fig. X | - |
| Density soil | $\rho_s$ | Fig. X | kg/m$^3$ |
| Shear wave velocity | $v_s$ | Fig. X | m/s |
| Damping ratio | $\zeta_s$ | 0.05 | - |

Table 3.3: Geometry and material properties of the soil.

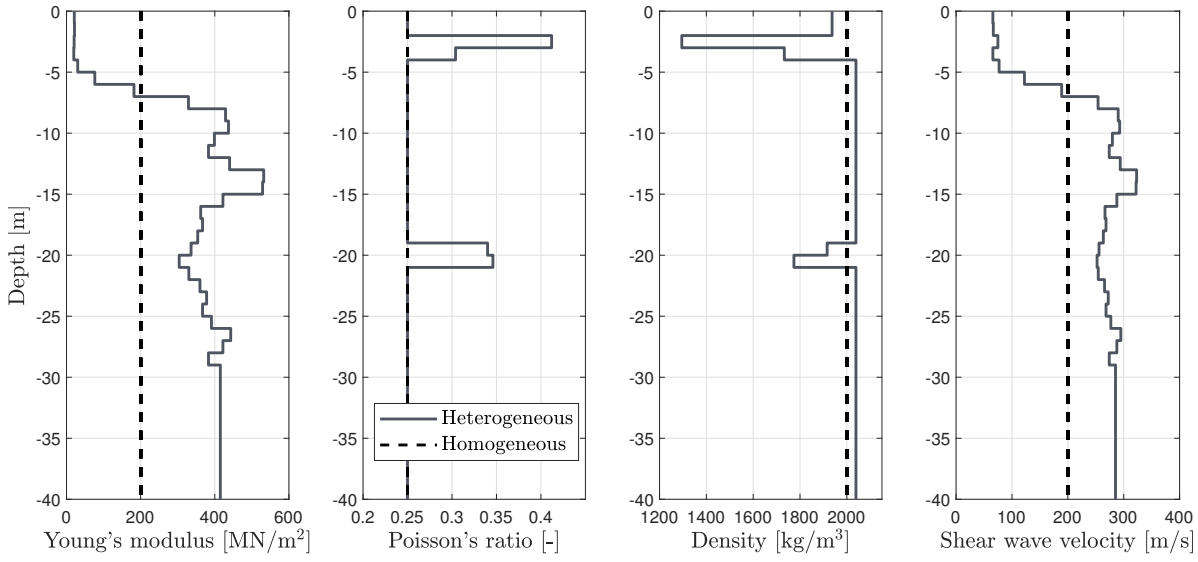


Figure 3.2: Young's modulus $E$, Poisson's ratio $\nu$, Density $\rho$ and shear wave velocity $v_s$ of the heterogeneous and homogeneous soil profile.

## 3.2. Numerical modelling

To solve the problem as introduced in the previous section, the finite element method is used. This numerical method subdivides the large continuous system into elements with finite dimension. The simple equations that model these finite elements are then assembled into a global system of equations that models the entire problem. The governing equations of the finite element analysis are described in section 3.2.1. Section 3.2.2 discusses the modelling of the seismic bedrock excitation and section 3.2.3 focuses on the important aspects of meshing, the domain size and the absorbing boundaries. Lastly, the 3D soil-structure model is validated by a comparative study with an open-source FE model called OpenSeesPL.

### 3.2.1. Governing equations

For the modelling of the linear elastic soil-structure system, cylindrical coordinates are used $(r,\theta,z)$. By applying the finite element method, the continuous physical problem is discretized into elements, interconnected at a finite number of nodes. Every node has three degrees of freedom; $u_r$, $u_\theta$ and $u_z$. The equations of motion of the obtained multi degree of freedom system can be formulated in the frequency domain as:

$$\mathbf{K}\mathbf{u} = \mathbf{f} \tag{3.2}$$

where $\mathbf{u}$ and $\mathbf{f}$ respectively contain amplitudes of nodal DOF and nodal load, and are a function of all three coordinates $(r,\theta,z)$. The global stiffness matrix $\mathbf{K}$ can be formulated as:

$$\mathbf{K} = \mathbf{K}_s + i\omega\mathbf{C} - \omega^2\mathbf{M} \tag{3.3}$$

The matrices $\mathbf{M}$, $\mathbf{C}$ and $\mathbf{K}_s$ represent the mass matrix, the damping matrix, and the static-stiffness matrix, which are constant for a linear system.

The geometry and material properties of the problem as introduced in section 3.1, exhibit symmetry around the $z$-axis. For the displacement boundary conditions, applied at the bottom boundary, this is not the case. Therefore, the problem is three-dimensional in the sense that every field quantity is a function of all three coordinates. However, it is possible to represent a load or displacement by components in the form of trigonometric series. Let the displacement amplitudes $\mathbf{u}$ be described as the sum of its series components:

$$\mathbf{u}(r,z,\theta,\omega) = \sum_{n=0}^{\infty} \mathbf{u}_n^c(r,z,\omega)cos(n\theta) + \sum_{n=0}^{\infty} \mathbf{u}_n^s(r,z,\omega)sin(n\theta) \tag{3.4}$$

where $\mathbf{u}_n^c$ and $\mathbf{u}_n^s$ are displacement amplitudes that depend on $n$, but not on $\theta$. In this type of representation completeness is preserved as the Fourier series can represent any continuous function within a given region. The forces can be described in a similar way:

$$\mathbf{f}(r,z,\theta,\omega) = \sum_{n=0}^{\infty} \mathbf{f}_n^c(r,z,\omega)cos(n\theta) + \sum_{n=0}^{\infty} \mathbf{f}_n^s(r,z,\omega)sin(n\theta) \tag{3.5}$$

Owing to the orthogonality principle it can be proven that the force term of the $n$th harmonic only affects the $n$th system of equations. This property allows us to solve only one set of equations if the Fourier expansion of the load involves only one term. If more terms are required to describe the problem, analysis can be performed for each component separately and results can be combined to produce the solution for the original loading. In this way, no division into elements in the $\theta$-direction is required, so that instead of solving the large 3D problem, several 2D problems can be solved. The system of algebraic equations describing the 2D problem for the $n$th harmonic can be described as:

$$\mathbf{K}_n\mathbf{u}_n = \mathbf{f}_n \tag{3.6}$$

in which $\mathbf{K}_n$, $\mathbf{u}_n$ and $\mathbf{f}_n$ are functions of two coordinates; $r$ and $z$. In this work, equation 3.6 is established and solved for $n = 0$ and $n = 1$.

### 3.2.2. Seismic boundary condition

In the seismic soil-structure problem, the load consist of the uniform harmonic excitation imposed at the bottom boundary of the soil domain. This is composed out of a vertical $(u_z^{br}(\omega))$ and horizontal component $(u_x^{br}(\omega))$. Separate analysis are required for the two components as the vertical component is described by terms independent of $\theta$ $(n = 0)$ and the horizontal component has a $\theta$-dependency described by first order

trigonometric terms ($n = 1$). Nodal amplitudes provided by the two separate analyses must be superposed to obtain the solution for the full loading situation.

First the vertical component is discussed. The loading state that imposes a vertical seismic excitation at the bottom boundary, while fixing the horizontal degrees of freedom of the rigid bedrock, is described by the following boundary conditions at $z = 0$:

$$u_r(r,\theta,0,\omega) = 0 \tag{3.7}$$
$$u_\theta(r,\theta,0,\omega) = 0 \tag{3.8}$$
$$u_z(r,\theta,0,\omega) = u_z^{br}(\omega) \tag{3.9}$$

Due to this loading character the displacement are independent of $\theta$:

$$u_r(r,\theta,z,\omega) = u_r(r,z,\omega) \tag{3.10}$$
$$u_\theta(r,\theta,z,\omega) = u_\theta(r,z,\omega) \tag{3.11}$$
$$u_z(r,\theta,z,\omega) = u_z(r,z,\omega) \tag{3.12}$$

The same holds for the internal stresses.

The uniform horizontal bedrock motion ($u_x^{br}$) can be decomposed into radial and circumferential components using first order trigonometric terms. In this loading state the vertical degrees of freedom of the rigid bedrock are fixed. The boundary conditions at $z = 0$ are described by:

$$u_r(r,\theta,0,\omega) = u_x^{br}(\omega)cos(\theta) \tag{3.13}$$
$$u_\theta(r,\theta,0,\omega) = u_x^{br}(\omega)sin(\theta) \tag{3.14}$$
$$u_z(r,\theta,0,\omega) = 0 \tag{3.15}$$

This loading character permits to describe the displacements and forces due to the horizontal bedrock motion, by making use of separation of variables. The $\theta$-dependencies for the displacements (and similarly for the stresses) are:

$$u_r(r,\theta,z,\omega) = u_r(r,z,\omega)cos(\theta) \tag{3.16}$$
$$u_\theta(r,\theta,z,\omega) = u_\theta(r,z,\omega)sin(\theta) \tag{3.17}$$
$$u_z(r,\theta,z,\omega) = u_z(r,z,\omega)cos(\theta) \tag{3.18}$$

To obtain the unknown field quantities, the boundary conditions at the bedrock DOFs need to be imposed into the global system of equations. Prescribing zero displacement boundary conditions at a specific nodal degree of freedom $k$, can be performed by removing the $k$th row and column in the dynamic stiffness matrix as well as the $k$th element in the force vector. Imposing non-zero displacement boundary conditions is less straightforward. To do this the system of equations needs to be decomposed into:

$$\begin{bmatrix} \mathbf{K}_{11} & \mathbf{K}_{12} \\ \mathbf{K}_{21} & \mathbf{K}_{22} \end{bmatrix} \begin{bmatrix} \mathbf{u}_f \\ \mathbf{u}_{br} \end{bmatrix} = \begin{bmatrix} \mathbf{f}_f \\ \mathbf{f}_{br} \end{bmatrix} \tag{3.19}$$

where $\mathbf{u}_{br}$ denote the imposed displacement amplitudes at the bedrock nodes and $\mathbf{f}_{br}$ the corresponding unknown nodal forces. The vector $\mathbf{u}_f$ contains the unknown nodal amplitudes of the remaining DOFs and the force vector of these DOFs is denoted with $\mathbf{f}_f$. By using this decomposition, the displacements $\mathbf{u}_f$ can then be determined by:

$$\mathbf{u}_f = \mathbf{K}_{11}^{-1}\left(\mathbf{f}_f - \mathbf{K}_{12}\mathbf{u}_{br}\right) \tag{3.20}$$

The vector containing the externally applied forces $\mathbf{f}_f$, has all components equal to zero if only the seismic loads introduced at the bedrock are considered.

### 3.2.3. Mesh and absorbing boundaries

The accuracy of the numerical approximation strongly depends on the size of the elements into which the system is discretized. For this reason, a mesh study is performed to optimize the dimension of the finite elements. Based on the accuracy of the results and the calculation time, an optimal mesh discretization is determined. The mesh size in the horizontal direction varies throughout the domain. Near the pile finite elements are used with a width equal to the thickness of the pile and towards the outer boundaries of the model, the mesh size gradually increases. The mesh is different for each case as the maximum element dimensions depend on the shortest wavelength present in the system. Based on the mesh study and recommendation in literature [37], the requirement is used that a full sinusoidal wave should at least be described by six elements. In the vertical direction, a constant discretization length of 0.5 meter is used. A finer mesh might still improve the numerical approximation, but the increase in computational demand due to the additional degrees of freedom does not outweigh the benefits in terms of accuracy.

Also the domain size and the absorbing boundaries play an important role in the accuracy of the numerical model. Inadequate consideration of these aspects may result in distortion of the systems dynamic characteristics and consequently inaccurate results. The use of finite elements in dynamic soil-structure problems requires special attention as soil layers of infinite extent in the horizontal direction must be represented by a model of finite size. For this purpose, absorbing boundaries are used at the outer boundaries of the system to satisfy the radiation condition.

A commonly applied method for truncating computational regions to simulate problems with open boundaries, makes use of Perfectly Matched Layers (PMLs) [15]. The principle behind this method is that the outwardly propagating waves enter a layer, where they are transformed into decaying evanescent waves to minimize the reflections at the boundary. The method introduces an absorbing layer with uniform thickness that forces the waves to decay exponentially. Note that this method is not developed for evanescent waves with complex-valued wavenumbers. PMLs are not effective in absorbing these types of waves, which may result in reflection [3]. Since evanescent waves decay automatically, an approach to prevent these reflections is choosing the domain size in such a way that the amplitudes of the evanescent waves are negligible at the start of the PML. For this reason the start of the absorbing PMLs is located at 30 times the length of the shortest shear wave present in the system. The PMLs are based on the properties of the soil continuum and the dimensions of the PMLs are determined such that 10 wavelengths fit in a PML. For more information about PMLs, the reader is advised to review [15].

### 3.2.4. Validation

To validate the model, results are compared with a different finite element model, computed in the software OpenSeesPL. In OpenSeesPL the linear elastic soil medium is modelled with 8-node brick elements and the pile is modelled as a one-dimensional beam. To account for the three-dimensional geometry of the embedded pile, the nodes of the 1D beam are connected to the nodes of the surrounding soil with very stiff beam elements. The static response of the MP foundation to a horizontal load is determined for the homogeneous soil case. It can be observed that the 3D models are in good agreement in both displacement $u(z)$ and rotation $\psi(z)$.

As an additional validation step the dynamic response of the soil system without pile is compared with that determined by a 1D shear wave propagation model of which the equation of motion was introduced in Equation 2.3. This is done to ensure adequate modelling of the seismic boundary condition. The homogeneous soil case is used and the load condition consists of a uniform horizontal bedrock motion with amplitude $u_x^{br}$. Both the real and imaginary part of the steady-state displacement are in good agreement for the frequency range of interest. The soil response for an excitation frequency of 1.5 Hz and 5.0 Hz is presented in Figure 3.3.

## 3.3. Response to seismic excitation

In this section a simulation of the 3D interaction between pile and soil is presented. First, the situation of the undisturbed soil is considered to give an impression of the seismic wave field generated by the bedrock motion. The steady-state response to a bedrock excitation with frequency of 5.0 Hz is presented in Figure 3.4 and 3.5. The figures clearly show the vertically propagating S-waves and P-waves, inducing a uniform ground motion along the horizontal plane. The figures also visualize the difference in wavelength between the two

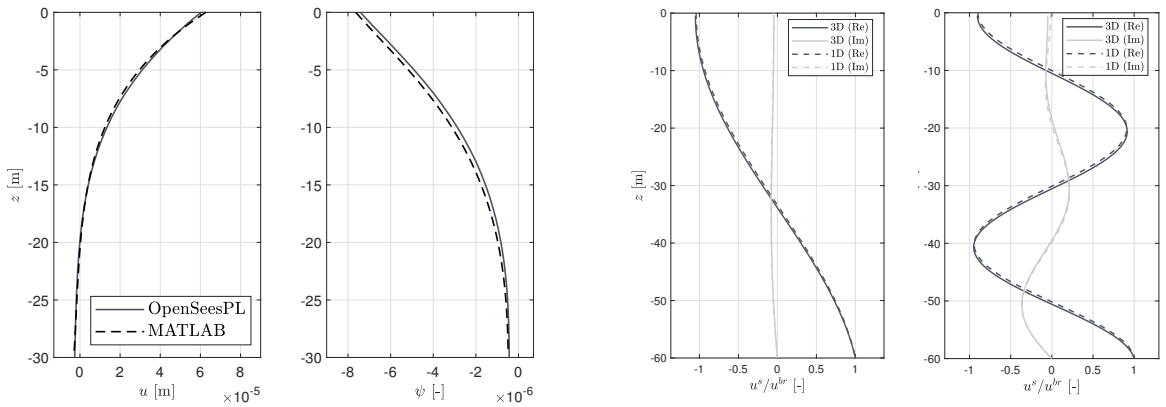


Figure 3.3: Validation of the 3D soil-structure model. *Left*: Pile response comparison between the MATLAB based FE model and the FE model computed in OpenSeesPL. A static horizontal force of 100 KN at 10 m above mudline is applied. *Right*: Undisturbed soil response comparison between the 3D FE model and 1D shear wave propagation model for uniform horizontal bedrock excitation with unit amplitude and frequencies of 1.5 Hz and 5.0 Hz.

types of body waves, as discussed in section 2.1. For the homogeneous soil, this wavelength is constant over the height, while the heterogeneous soil shows an irregular response due to the varying elastic properties. Furthermore, the amplification of the seismic bedrock motion is analyzed. In Figure 3.8, the amplitude ratio between bedrock displacement and ground surface displacement is presented for both vertical and horizontal motion. This is done for the homogeneous and heterogeneous soil deposit. The seismic motion is significantly amplified for frequencies corresponding to the resonance of the soil stratum for vertical S-wave propagation and vertical P-wave propagation.

When including the monopile-based offshore wind turbine, a disturbance of the ground motion is introduced. This is visualized in Figure 3.6 and 3.7. The system with structure is subjected to the same bedrock motion as considered for the soil-only case (Figure 3.4 and 3.5). The disturbance of the seismic wave field arise from the following processes: Due to the sudden change in elastic properties at the soil-pile interface phenomena such as scattering, refraction and diffraction occur, causing seismic energy to be deflected in different directions. Part of the seismic energy is transmitted to the foundation which induces structural vibrations. The inertia forces that are subsequently generated in the superstructures mass, produce dynamic forces. These forces are transmitted onto the foundation and eventually in the surrounding soil, causing additional ground displacements. Figure 3.6 and 3.7 also visualize the mode conversion of the incoming body waves to waves travelling along the soil surface.

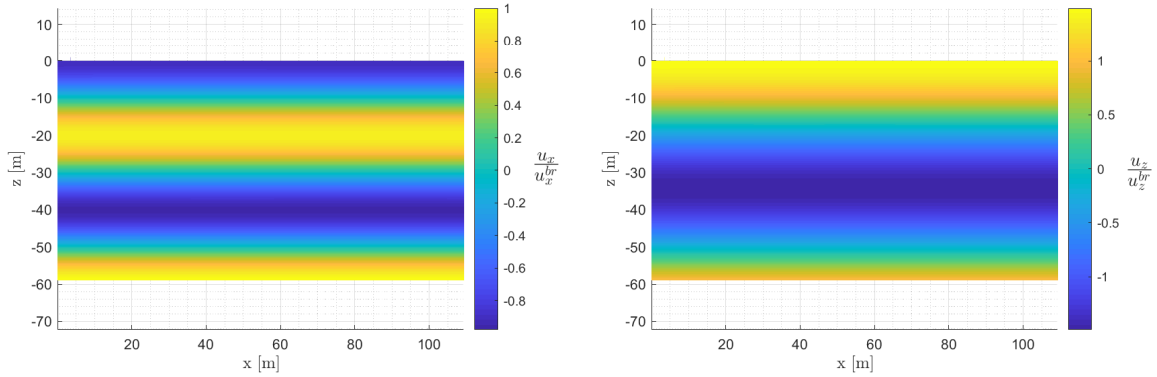


Figure 3.4: The steady-state response of the homogeneous soil deposit without structure, in the x- and z-direction. Induced by a uniform vertical and horizontal bedrock excitation with unit amplitude and frequency 5.0 Hz.

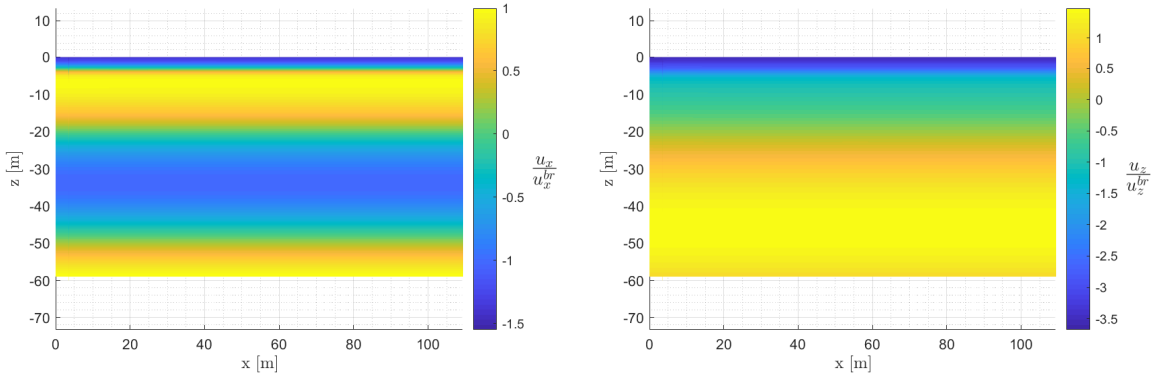


Figure 3.5: The steady-state response of the heterogeneous soil deposit without structure, in the x- and z-direction. Induced by a uniform vertical and horizontal bedrock excitation with unit amplitude and frequency 5.0 Hz.

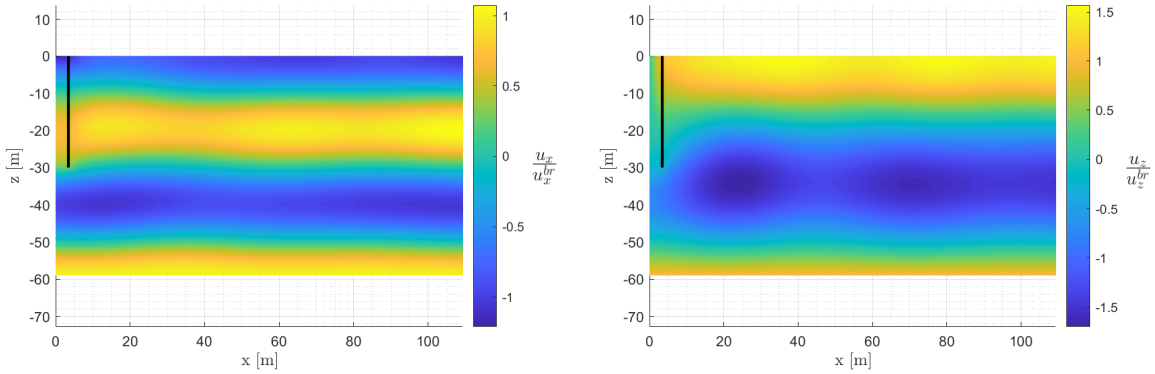


Figure 3.6: The steady-state response of the homogeneous soil with structure, due to a uniform vertical and horizontal bedrock excitation with unit amplitude and frequency 5.0 Hz.

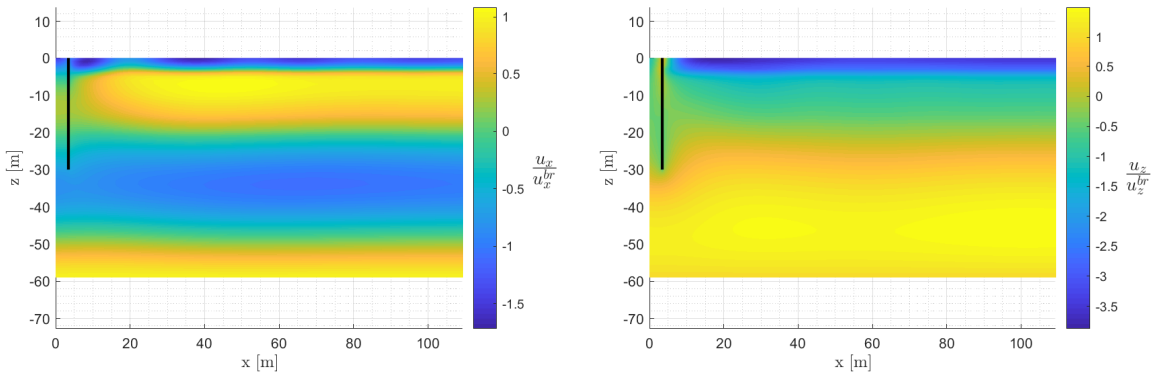


Figure 3.7: The steady-state response of the heterogeneous soil with structure, due to a uniform vertical and horizontal bedrock excitation with unit amplitude and frequency 5.0 Hz.

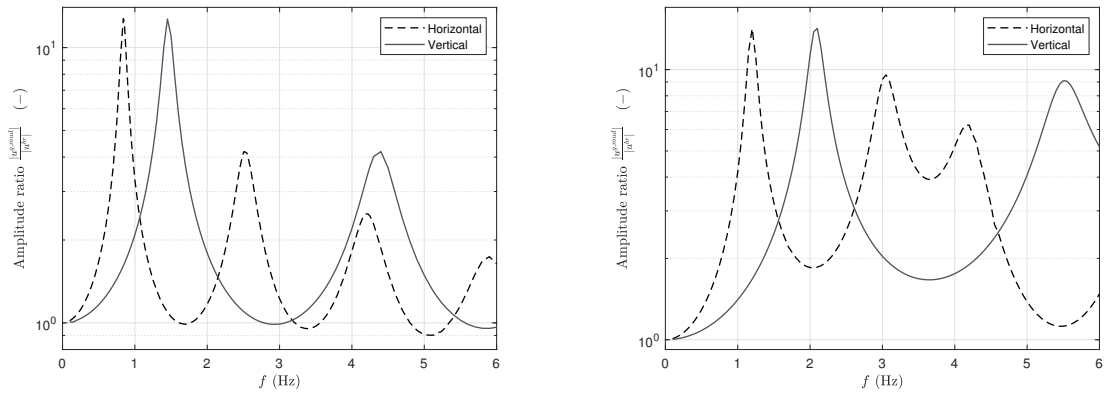


Figure 3.8: Frequency response function of the soil deposit without structure. The amplitude ratio between bedrock and mudline displacement is displayed for the homogeneous (*left*) and heterogeneous (*right*) soil profile.

# 4

# Effective 1D model

Along with the development of rigorous modelling methods, comes the need to translate the response of those models into simplified, effective models. Effective modelling methods are particularly important for the design of offshore wind turbines as the stochastic loading environment of these structures requires a great number of time-domain simulations. In such a design process, it is of great value to reduce the number of DOF by using simplified models, provided that it has been shown to match the rigorous results adequately. For these reasons the main objective of this work is to *establish a method to identify an effective 1D model for seismic analysis of monopile-based offshore wind turbines that incorporates 3D soil-structure interaction.* This objective will be addressed in this chapter.

The approach as established in this work is based on the Beam-on-dynamic-Winkler-foundation (BDWF) model, in which the soil is represented by springs and dashpots continuously distributed along the embedded pile. The BDWF modelling approach has been used extensively to estimate the soil reaction for monopile-based offshore wind turbines subjected to hydrodynamic and aerodynamic loads. However, specific for seismic action is that it originates from the soil and therefore the load itself is developed due to soil-structure interaction. This requires an additional step in establishing an effective 1D Winkler-type model, namely, determining and incorporating the effective seismic excitation. In this thesis a substructuring approach is used for this purpose. A generic formulation of this substructuring approach will be presented in Section 4.1. Subsequently, in Section 4.2, the expression found to describe the soil-structure interaction forces is explained. Section 4.3 to 4.5 elaborates on the applied procedure to obtain the 1D model and in Section 4.6 the numerical implementation is discussed.

## 4.1. Substructuring method of analysis

For the design of OWT support structures the response of the structure itself is of primary interest and an equivalent representation of the soil reaction with proper consideration of the seismic input, usually suffices. Therefore, the approach used to establish the effective model for seismic analysis of offshore wind turbines is based on dynamic substructuring. By adopting this approach, the seismic load simulations of the complex wind turbine structure can be performed without explicitly modelling the soil. This is a highly favourable approach as modelling of the soil domain is complicated and it increases the computational time significantly.

In this section, a generic mathematical formulation of the dynamic substructuring approach is provided for a multi-degree-of-freedom structural system with an embedded foundation. This formulation is based on the work of Wolf [35]. The approach is based on subdividing the fully coupled system into two separate substructures; the structure itself and the soil with excavation. The components are joined at the common interface by imposing force equilibrium conditions and kinematic compatibility at all times. In Section 4.3, the substructuring method of analysis is applied to establish the 1D effective model.

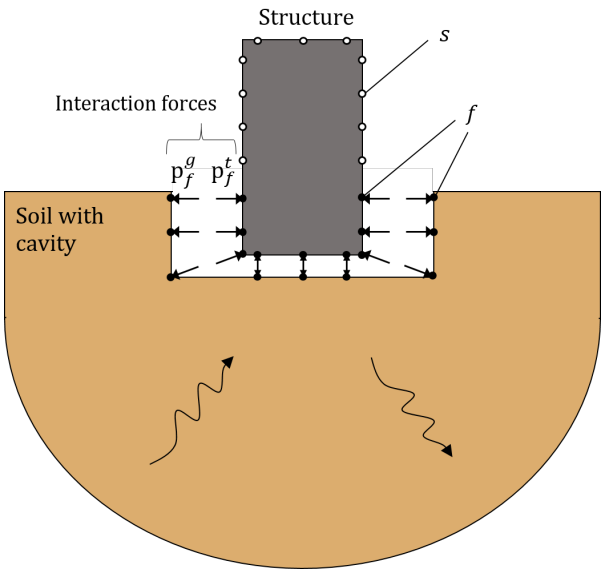


Figure 4.1: A visualization of the substructuring method of analysis.

The first step of the substructuring approach is formulating the equations of motion of the MDOF structural system. This is done in a partitioned form, by distinguishing between DOFs of the foundation (subscript $f$) - which are in contact with the soil - and the remaining structural DOFs (subscript $s$). When only considering seismic loads, the nodes not in contact with the soil are not externally loaded. Under this assumption, the response of the structure is only induced by the interaction forces with the soil and therefore the structural response is denoted as the "total" response (superscript "t"). The system of equations describing the equilibrium of the structure can be formulated in the frequency domain as:

$$\begin{bmatrix} \mathbf{K}_{ss} & \mathbf{K}_{sf} \\ \mathbf{K}_{fs} & \mathbf{K}_{ff} \end{bmatrix} \begin{bmatrix} \mathbf{u}_s^t \\ \mathbf{u}_f^t \end{bmatrix} = \begin{bmatrix} \mathbf{0} \\ \mathbf{p}_f^t \end{bmatrix} \tag{4.1}$$

In equation 4.1 the following notations are used:

- $\mathbf{K}_{ss}$, $\mathbf{K}_{sf}$, $\mathbf{K}_{fs}$ and $\mathbf{K}_{ff}$: the submatrices forming the dynamic stiffness matrix of the structure. Subscript "s" refers to the structural while "f" to the foundation DOFs, namely the ones positioned at the soil-structure interface.
- $\mathbf{u}_s^t$: displacement vector of the DOFs of the structure, excluding the ones positioned at the interface.
- $\mathbf{u}_f^t$: vector of displacements of the foundation DOFs; the ones at the soil-structure interface.
- $\mathbf{p}_f^t$: total nodal interaction forces developed at the soil-structure interface.

Besides the structural subsystem, also the soil subsystem contributes to the equilibrium of the nodes located at the soil-structure interface, through interaction forces $\mathbf{p}_f^t$. In order to obtain these unknown interaction forces, the two substructures should be assembled by applying two interface conditions. The first condition is force equilibrium, which states that the interface stresses between connecting nodes should have equal magnitude and opposing sign. The nodal interaction forces acting on the structure ($\mathbf{p}_f^t$) and those acting on the soil subsystem ($\mathbf{p}_f^g$), can thus be related by the following equation:

$$\mathbf{p}_f^t(\omega) = -\mathbf{p}_f^g(\omega) \tag{4.2}$$

The second interface condition is coordinate compatibility; as the foundation and the soil are perfectly bonded at the contact surface the connecting nodes of the two substructures should have equal interface displacement:

$$\mathbf{u}_f^t(\omega) = \mathbf{u}_f^g(\omega) \tag{4.3}$$

As a linear system is considered, the response of the soil substructure can be decomposed into multiple loading components. These can be determined individually and the total response can be found by superposition of the separate components. In this case two loading states are considered. The first includes the response induced by the earthquake action. In this loading state, the seismic excitation is imposed at the bedrock boundary while the complete soil surface, including cavity surface, is free of stress.

The second component is the response induced by the interaction stresses with the structure, acting on the surface of the cavity. In this case the bottom boundary of the soil subsystem is fixed and no incident wave field is present. The total displacement of the nodes on the interface, can now be formulated as:

$$\mathbf{u}_f^t(\omega) = \mathbf{u}_f^{g,i}(\omega) + \mathbf{u}_f^{g,e}(\omega) \tag{4.4}$$

The vector $\mathbf{u}_f^{g,e}$ denotes the displacement amplitudes of the soil subsystem due to the earthquake component, for the nodes located at the cavity surface. Vector $\mathbf{u}_f^{g,i}$ denotes the displacements of the same nodes due to the soil-structure interaction forces.

The forces acting on nodes $f$ can be partitioned by making use of the same two loading states:

$$\mathbf{p}_f^t(\omega) = -\mathbf{p}_f^{g,i}(\omega) \underbrace{-\mathbf{p}_f^{g,e}(\omega)}_{=0} \tag{4.5}$$

where, $\mathbf{p}_f^{g,i}$ are the forces acting on the nodes $f$ of the soil subsystem, due to the SSI and the vector $\mathbf{p}_f^{g,e}$ denotes the forces on the same nodes $f$, due to the seismic excitation imposed upon the soil subsystem. The latter are equal to zero as the cavity surface is stress-free for the earthquake loading state. Therefore, the total nodal forces at the interface merely consists of the ones originating due to the soil-structure interaction component.

Let $\mathbf{G}_{ff}$ be the dynamic stiffness matrix of the soil substructure, describing the relation between force and displacement of all nodes on the cavity surface. Then the displacement of nodes $f$ of the soil subsystem due to the forces $\mathbf{p}_f^{g,i}$ can be determined by:

$$\mathbf{u}_f^{g,i}(\omega) = \mathbf{G}_{ff}^{-1}\mathbf{p}_f^{g,i}(\omega) \tag{4.6}$$

By making use of equation 4.4 and 4.5, this can be rewritten to:

$$\mathbf{p}_f^t(\omega) = \mathbf{G}_{ff}\left(\mathbf{u}_f^{g,e}(\omega) - \mathbf{u}_f^t(\omega)\right) \tag{4.7}$$

which can be implemented in equation 4.1:

$$\begin{bmatrix} \mathbf{K}_{ss} & \mathbf{K}_{sf} \\ \mathbf{K}_{fs} & \mathbf{K}_{ff} + \mathbf{G}_{ff} \end{bmatrix} \begin{bmatrix} \mathbf{u}_s^t(\omega) \\ \mathbf{u}_f^t(\omega) \end{bmatrix} = \begin{bmatrix} \mathbf{0} \\ \mathbf{G}_{ff}\mathbf{u}_f^{g,e}(\omega) \end{bmatrix} \tag{4.8}$$

Once the complex-valued soil stiffness matrix $\mathbf{G}_{ff}$ and the seismic input $\mathbf{u}_f^{g,e}$ are determined by using the soil subsystem, this can be implemented in the structural model to determine the structural response to earthquake loading. The size of the dynamic soil stiffness matrix is $m \times m$, with $m$ being the number of degrees of freedom of nodes located on the soil-structure interface. Matrix $\mathbf{G}_{ff}$ includes both diagonal and non-diagonal terms as the response of a soil continuum is in general coupled and non-local. In continuous systems the stiffness matrix $\mathbf{G}_{ff}$ may be formulated as a linear operator $G_{ff}$. Any type of solution method can be used to capture the force-displacement relation of the soil subsystem at the contact surface with the structure. It may be a semi-analytical solution approach - for instance, using Greens's functions - or a numerical one. In the current work, $\mathbf{G}_{ff}$ is captured using a soil subsystem modelled as a 3D continuum with finite elements. This approach, based on the work of Versteijlen [30, 31], will be discussed in the coming sections.

## 4.2. Seismic soil-structure interaction forces

Before establishing the effective 1D model using the substructuring method of analysis, the obtained relation for the soil-structure interaction forces acting on the foundation (Eq. 4.7) is explained. The total interaction forces between the soil and structure are a superposition of the following two components:

$$\mathbf{p}_f^t = \mathbf{p}_f^I + \mathbf{p}_f^{II} \tag{4.9}$$

where the forces $\mathbf{p}_f^I$ and $\mathbf{p}_f^{II}$ are defined as:

$$\mathbf{p}_f^I = \mathbf{G}_{ff}\,\mathbf{u}_f^{g,e} \tag{4.10}$$

$$\mathbf{p}_f^{II} = -\mathbf{G}_{ff}\,\mathbf{u}_f^t \tag{4.11}$$

The loading component $\mathbf{p}_f^I$ introduces the seismic action to the system and is therefore referred to as the excitation load. This loading component is generated by incoming seismic waves interacting with the stationary structural body and is therefore independent of the motion of the structure. It can be decomposed into a free-field component and a diffraction component, as is commonly done in the field of hydrodynamics to determine wave forces acting on a body [21]. The theoretical prove that the excitation load as defined in this work, captures the free-field as well as the diffracted component is included in Appendix B. This appendix also elaborates on the analogy with the hydrodynamic approach. The loading state corresponding to the excitation component of the soil-structure interaction force is visualized in Figure 4.2.

The interaction forces developed due to the motion of the structure are captured in the component $\mathbf{p}_f^{II}$. This force component - referred to as the radiation force - can be interpret as the force originating due to the structural vibrations in the absence of ground motion induced by incoming seismic waves. This is depicted in Figure 4.2. When only earthquake loads are considered, the structural motion is fully induced by the seismic excitation load ($\mathbf{p}_f^I$) and, thus, no SSI forces would develop in the absence of earthquake ground motion.

Now that the SSI forces during seismic loading are defined, the assumption behind the conventional modelling procedures using free-field ground motion in a Winkler-type foundation model, can be identified. In determining the earthquake ground motion, these engineering modelling methods do not account for diffraction because of the geometrical irregularity introduced into the soil deposit by the embedded part of the structure. Therefore, the excitation load considered in these methods, does not account for the diffracted wave force component.

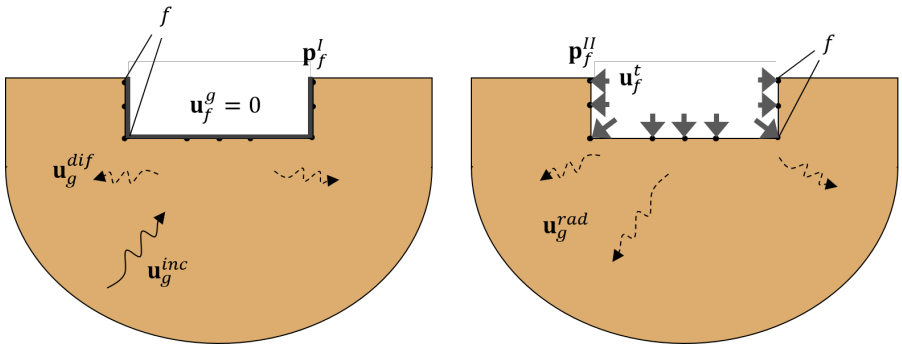


Figure 4.2: A graphical presentation of the two loading components that together represent the total interaction forces between soil and structure. The excitation load ($\mathbf{p}_f^I$) is shown left and the inertial load ($\mathbf{p}_f^{II}$) on the right.

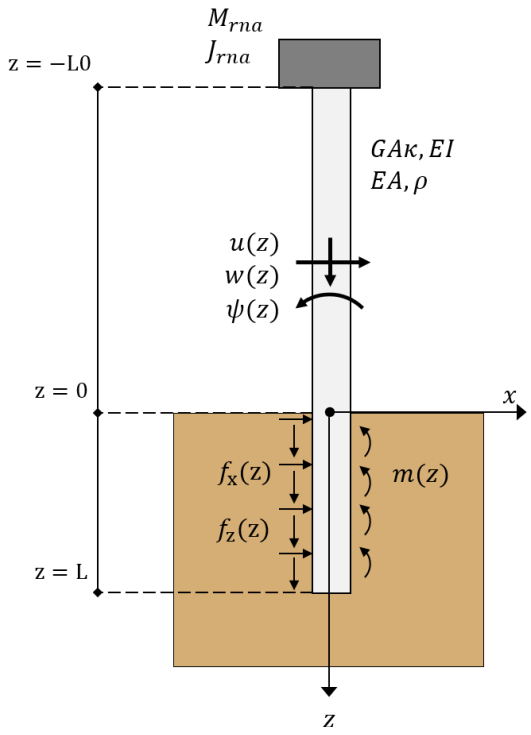


Figure 4.3: Graphical representation of the 1D beam model with soil-structure interaction forces.

## 4.3. Governing equations of the 1D model

With the substructuring method as introduced in the previous section, the 1D model for seismic analysis of monopile based OWTs can be established. This modelling approach provides a substructure in the form of a Winkler foundation stiffness matrix, along with the effective seismic input, represented by a ground motion signal along the embedded length of the monopile. These soil related components are incorporated in the structural model to introduce the seismic action and account for SSI effects. Extraction of the dynamic soil stiffness matrices and the seismic input motion, by using the soil substructure model, is discussed in Section 4.4 and 4.5. First, the governing equations of the 1D SSI system are introduced in Section 4.3.

The first step of the substructuring method is to establish the equations of motion of the structure. The Timoshenko beam theory is used for this purpose, as it was found that both shear deformation and rotational bending effects should be accounted for to describe the 3D response of large diameter piles. The equilibrium equations of a Timoshenko beam, representing a monopile with external distributed forces are:

$$GA\kappa\left(\frac{d^2u(z)}{dz^2} - \frac{d\psi(z)}{dz}\right) + \omega^2\rho Au(z) = f_x(z,\omega) \tag{4.12}$$

$$GA\kappa\left(\frac{du(z)}{dz} - \psi(z)\right) + EI\frac{d^2\psi(z)}{dz^2} + \omega^2\rho I\psi(z) = m(z,\omega) \tag{4.13}$$

where equation 4.12 describes the balance of lateral forces, and equation 4.13 describes the balance of bending moments. Both are formulated in the frequency domain. $GA\kappa$ is the product of the steel shear modulus $G$, the cross-sectional area $A$ and the cross section-dependent shearing coefficient $\kappa$. For the cylindrical pile section, $\kappa = 0.53$ is assumed. Furthermore, $EI$ is the product of the steel Young's modulus $E$ and the second moment of area of the cross section of the pile $I$.

To include vertical degrees of freedom in the 1D model, an additional equation of motion is introduced for equilibrium in the z-direction. This formulation is based on a simple rod in axial motion. The equation of motion describing the longitudinal motion is:

$$EA\frac{d^2w(z)}{dz^2} + \omega\rho Aw(z) = f_z(z,\omega) \tag{4.14}$$

In equations 4.12 - 4.14, $f_x$, $m$ and $f_z$ are respectively the distributed lateral force, bending moment and vertical force due to soil-structure interaction. These interaction forces introduce the seismic load to the structure. The geometry and sign convention of the 1D model is presented in Figure 4.3. In establishing the equations of motion, the assumption is made that there is no coupling effect between the axial motion of the structure and the rotational and lateral motion.

The boundary conditions as used in the model are given below. The first three incorporate the RNA mass at tower top and the equations 4.18 to 4.20 prescribe the free-end conditions at pile tip.

$$GA\kappa\left(\frac{du(z)}{dz}-\psi(z)\right)\Big|_{z=-L_0} = -\omega^2 M_{RNA}u(0) \tag{4.15}$$

$$EI\frac{d\psi(z)}{dz}\Big|_{z=-L_0} = -\omega^2 J_{RNA}\psi(0) \tag{4.16}$$

$$EA\frac{dw}{dz}\Big|_{z=-L_0} = -\omega^2 M_{RNA}w(0) \tag{4.17}$$

$$GA\kappa\left(\frac{du(z)}{dz}-\psi(z)\right)\Big|_{z=L} = 0 \tag{4.18}$$

$$EI\frac{d\psi(z)}{dz}\Big|_{z=L} = 0 \tag{4.19}$$

$$EA\frac{dw}{dz}\Big|_{z=L} = 0 \tag{4.20}$$

Next, the contribution of the soil substructure to the equilibrium of the structure will be incorporated. This will be done by introducing the dynamic soil stiffness according to equation 4.8, by making use of the global stiffness operator $G_{ff}$. As discussed in section 4.1, this operator describes the relation between soil reaction force and displacement at the soil-structure interface. Because the displacement of the beam is described by the three components, $u$, $\psi$ and $w$, it is convenient to decompose $G_{ff}$ into the sub-operators $K^{u,u}$, $K^{\psi,\psi}$, $K^{w,w}$, $K^{u,\psi}$ and $K^{u,\psi}$. The soil stiffness operators coupling $w$ to $u$ and $\psi$ are not considered in this work, because the assumption is made that the axial motion of the system is uncoupled from the lateral and rotational motion.

Besides introducing the dynamic soil stiffness operators, also the effective seismic input is introduced into the equilibrium equations of the structure. In the 1D effective modelling approach established in this work, the seismic input is represented by the motion of the soil substructure due to the seismic excitation. This motion is determined for the line that forms the interface between the soil and structure and is described by the components $u_g(z)$, $\psi_g(z)$ and $w_g(z)$.

Upon incorporating the contribution of the soil subsystem according to equation 4.8, the interaction forces $f_x$, $m$ and $f_z$ in the equilibrium equations (Eq. 4.12, 4.13 and 4.14) become integrals:

$$GA\kappa\left(\frac{d^2u(z)}{dz^2}-\frac{d\psi(z)}{dz}\right)+\omega^2\rho Au(z)-\int_0^L K^{u,u}(z,\bar{z})u(\bar{z})d\bar{z}-\int_0^L K^{u,\psi}(z,\bar{z})\psi(\bar{z})d\bar{z} = -\int_0^L K^{u,u}(z,\bar{z})u_g(\bar{z})d\bar{z}-\int_0^L K^{u,\psi}(z,\bar{z})\psi_g(\bar{z})d\bar{z} \tag{4.21}$$

$$GA\kappa\left(\frac{du(z)}{dz}-\psi(z)\right)+EI\frac{d^2\psi(z)}{dz^2}+\omega^2\rho I\psi(z)-\int_0^L K^{\psi,\psi}(z,\bar{z})\psi(\bar{z})d\bar{z}-\int_0^L K^{\psi,u}(z,\bar{z})\psi(\bar{z})d\bar{z} = -\int_0^L K^{\psi,\psi}(z,\bar{z})\psi_g(\bar{z})d\bar{z}-\int_0^L K^{\psi,u}(z,\bar{z})\psi_g(\bar{z})d\bar{z} \tag{4.22}$$

$$EA\frac{d^2w(z)}{dz^2}+\omega^2\rho Aw(z)-\int_0^L K^{w,w}(z,\bar{z})w(\bar{z})d\bar{z} = -\int_0^L K^{w,w}(z,\bar{z})w_g(\bar{z})d\bar{z} \tag{4.23}$$

In these equations of motion, the terms on the right hand side introduce the earthquake action to the structure. Note that the interaction force between soil and pile at a location $z$, is a function of the pile displacement at that particular location *and* the pile displacements at all other locations along the embedded part of the pile. This is due to the non-local effects included in this modelling method. Although the integral only captures the domain from mudline to pile tip, the interaction forces between the soil and structure are the reaction of the whole soil continuum. This is implicitly included in determining the dynamic soil stiffness kernels.

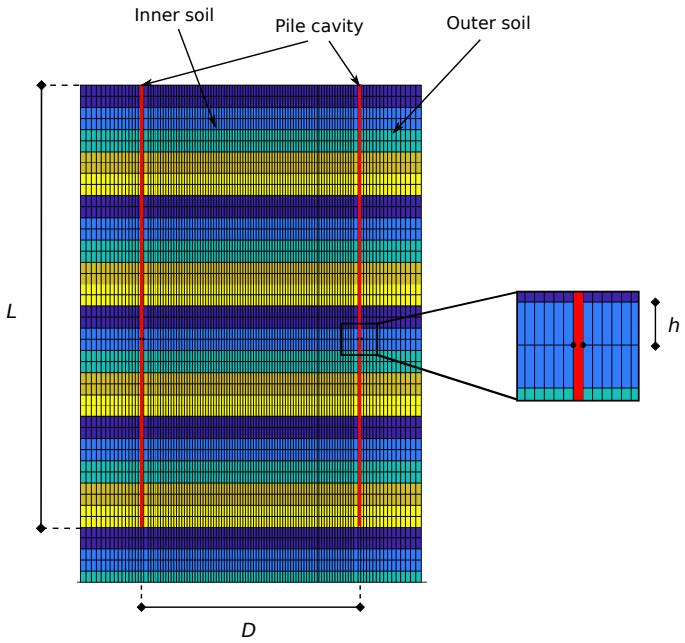


Figure 4.4: A graphical presentation of the FE mesh of the soil substructure model, with the pile cavity in red. Only a small section around the pile is shown.

## 4.4. Extracting the 3D continuum reaction

To determine the dynamic soil stiffness matrices required for the one-dimensional BDWF model, the non-local method as established by Versteijlen is used. In the non-local method, the complex, global soil reactions are extracted from a linear elastic 3D soil model and inserted in a 1D Winkler-type model. The method was shown to yield accurate fits of both the static and low-frequency dynamic response for a large range of soil-structure interaction problems.

The 3D model used to extract the dynamic soil stiffness matrices is based on the model introduced in Chapter 3. The structure is removed to obtain the soil subsystem model, which includes a cavity at the location of the MP. As the steel tubular structure itself is not included, the terms of the soil stiffness matrix do not depend on the material properties of the MP foundation, but only on it's geometry. When using a numerical solution method, the stiffness operators, as introduced in section 4.3, will be discretized into stiffness matrices of size $n \times n$, with $n$ the amount of nodes used to discretize the 1D structural model. The methodology to determine the sub-matrices $\mathbf{K}^{u,u}$, $\mathbf{K}^{\psi,\psi}$, $\mathbf{K}^{\psi,u}$, $\mathbf{K}^{u,\psi}$ and $\mathbf{K}^{w,w}$, is briefly described below. For further background about the extraction of the non-local stiffness kernels reference is made to the work of Versteijlen [31].

Capturing the sub-matrix $\mathbf{K}^{u,u}$ is done using the following procedure; for every discrete depth $z_i$ the circumferential ring of nodes of the cavity surface is displaced with a certain amplitude $u_i$ in the x-direction. The prescribed displacement amplitudes are collected in the matrix $\mathbf{U}_x$, which is a diagonal matrix. Next, the sum of the nodal horizontal reaction forces is collected at that ring as well as for all the other vertically spaced rings, at depths $z_{j\neq i}$. A matrix $\mathbf{F}_x$ is constructed from column vectors $f_{x,j}$, being the reaction forces at depths

$z_j$ due to the displacements at depths $z_i$. With the matrices $\mathbf{F}_x$ and $\mathbf{U}_x$, the soil stiffness matrix $\mathbf{K}^{u,u}$ can be determined by making use of equation 4.24.

$$\mathbf{K}^{u,u} = \frac{\mathbf{F}_x \tilde{\mathbf{U}}_x^{-1}}{h} \tag{4.24}$$

In Eq. 4.24, the nodal force matrix $\mathbf{F}_x$ is divided by the discretisation length $h$ as the unit of the lateral equilibrium forces (Eq. 4.21) is N/m. Moreover, the tilde over the matrix $\mathbf{U}_x$ indicates that it is an auxiliary matrix that incorporates the trapezium rule of integration. This is done in order to be consistent with the integral in equations 4.21.

Along this line, the rotational stiffness matrix $\mathbf{K}^{\psi,\psi}$, can be found by imposing a rotation $\psi_i$ on the nodal rings along the circumference of the cavity surface, collecting the nodal reaction forces in vertical direction for all depths, and thus form the matrix $F_z$. The lever arm of the vertical reaction forces is incorporated ($D/2$) as $\mathbf{K}^{\psi,\psi}$ relates the rotations to the distributed moment.

$$\mathbf{K}^{\psi,\psi} = \frac{D\mathbf{F}_z \tilde{\Psi}^{-1}}{2h} \tag{4.25}$$

in which $\tilde{\Psi}$ is the matrix containing the imposed rotation (including the trapezium rule of integration). The stiffness matrix coupling the lateral soil reaction to rotations is determined by:

$$\mathbf{K}^{u,\psi} = \frac{\mathbf{F}_x \tilde{\Psi}^{-1}}{h} \tag{4.26}$$

$$\tag{4.27}$$

and the matrix coupling the rotational reaction to lateral displacements of the nodal rings by:

$$\mathbf{K}^{\psi,u} = \frac{D\mathbf{F}_z \tilde{\mathbf{U}}_x^{-1}}{2h} \tag{4.28}$$

To capture the matrix $\mathbf{K}^{w,w}$, a vertical displacement of the ring of nodes is imposed for every depth $z_i$ and the vertical nodal reaction forces are collected along the circumference of the cavity. The stiffness matrix can then be found as

$$\mathbf{K}^{w,w} = \frac{\mathbf{F}_z \tilde{\mathbf{U}}_z^{-1}}{h} \tag{4.29}$$

Due to the axisymmetry of the vertical displacement imposed to every ring of nodes, there is no resultant lateral force or bending moment acting on the pile. Therefore, no soil stiffness matrices coupling $w$, to $u$ and $\psi$ are extracted.

## 4.5. Effective seismic input

Besides using the 3D FE model of the soil subsystem for capturing the dynamic soil stiffness matrices, this model will also be used to extract the seismic input required for the 1D modelling approach. This seismic input is defined by the motion of the soil substructure due to the earthquake action introduced at the bedrock boundary. As discussed in section 4.1, only the motion of the surface that forms the soil-structure interface is required. Because the monopile is not present in this substructuring step, the interface surface - also referred to as the excavation or cavity surface - is stress-free. The presence of the excavation leads to a discontinuity of the soil body and therefore the response of the soil subsystem will differ from the free-field ground response. The excavation alters the incident wave front and seismic energy is deflected in different directions due to phenomena known as wave diffraction or scattering. For this reason, the earthquake motion of the soil body with cavity is referred to as the disturbed or scattered ground motion.

The scattered ground motion is a result of 3D modelling and is thus a function of three spatial coordinates. However, the ground motion required for the 1D modelling approach is characterized by $u_g(z)$, $\psi_g(z)$ and $w_g(z)$, which only vary in the vertical direction. Therefore, this substructuring step must be performed in such a way that the scattered motion of the cavity can be described as a function of time and $z$ only. For the

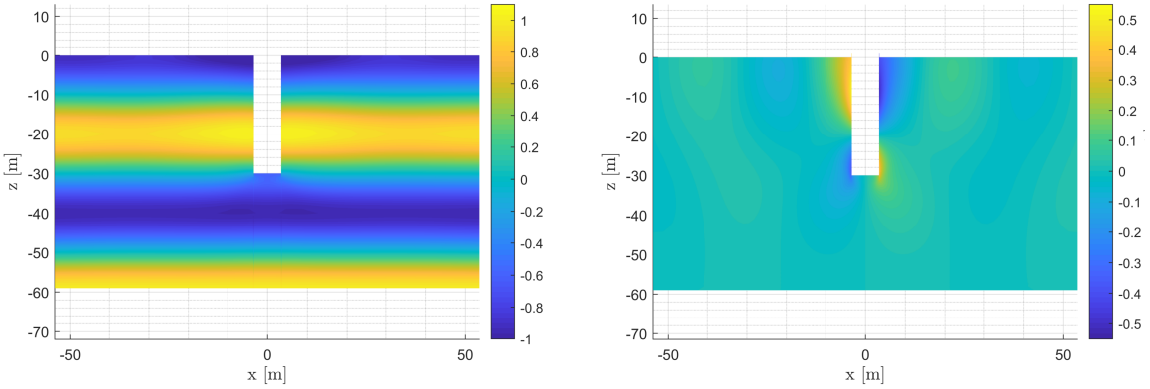


Figure 4.5: An impression of the ground motion of the soil subsystem witch excavation. The steady-state response to a harmonic horizontal bedrock motion with unit amplitude and $f = 5.0$ Hz is shown, for Case 1A (homogeneous soil profile and no soil inside MP). On the left the displacement in the x-direction is presented and on the right the displacement in the z-direction.

situation without soil inside the pile, this is relatively straightforward, as in this case the interface between soil and structure only consists of the outside cavity surface. To obtain the displacements ($u_g$, $\psi_g$ and $w_g$) as a function of one spatial coordinate only, the motion of each ring of nodes located on this outer surface is simply averaged. The assumption behind this approach is that under the given loading conditions, the ovalization of the cavity circumference can be disregarded and does not affect the seismic loads transmitted to the structure. An impression of the scattered ground motion is presented for the homogeneous soil profile in Figure 4.5. The seismic environment is generated by a uniform horizontal bedrock motion with unit amplitude. No vertical component is included. It shows that the vertically propagating shear waves are affected by the presence of the excavation and that these waves do not only impose a lateral displacement to the cavity but also a rotation due to the varying z-displacements. When also vertical seismic bedrock motion would be included, the cavity would experience an additional vertical displacement.

For the cases with soil inside the tubular monopile section, two rings are present along the embedded pile length; the inner ring and the outer ring. Together these rings form the cavity surface, as depicted in Figure 4.4. Simply averaging the motion of the two rings at each level of $z$, does not provide an accurate representation. The response of the inner soil differs significantly from the outer soil due to the locally varying dynamic response. This is not accounted for in extracting the dynamic stiffness kernels, which are based on the assumption that the a pile section behaves as a rigid disk and therefore no distinction is made between the stiffness contribution of the soil inside and outside of the monopile. As a solution the DOF of the inner nodes and outer nodes are coupled when determining the response of the soil subsystem, such that the inner ring at level $z$ has the same horizontal displacement, rotation and vertical displacement as the outer ring. This implies that each section of the excavation behaves as a rigid disk - an assumption similar to the one applied to extract the soil impedance from the 3D model. When applying this restriction additional (non-physical) forces are introduced and the cavity surface is no longer a stress-free surface. It is however verified that these forces can be neglected with respect to the forces induced by the motion of the structure.

## 4.6. Numerical implementation

To numerically approximate the solution of the dynamically loaded Timoshenko beam on a non-local Winkler foundation, the central finite difference method is used. The MATLAB based numerical model used in this work is a modification of the model used by Versteijlen [31]. Using the finite difference method, the functions $u(z)$, $\psi(z)$ and $w(z)$ are evaluated in a domain of length $L+L_0$ at $n$ equally spaced points. The discretisation length is $h = (L+L_0)/(n-1)$. Using this schematization, the first and second derivative terms of equations 4.12 - 4.14 are approximated. Using Einstein summation convention the equations of motion can be formulated:

$$\frac{GA\kappa}{h^2}(u_{i-1}-2u_i+u_{i+1})-\frac{GA\kappa}{2h}(-\psi_{i-1}+\psi_{i+1})+\omega^2\rho A u_i-\tilde{K}^{u,u}_{i,j}u_j-\tilde{K}^{u,\psi}_{i,j}\psi_j=-\tilde{K}^{u,u}_{i,j}u^g_j-\tilde{K}^{u,\psi}_{i,j}\psi^g_j \quad (4.30)$$

$$\frac{GA\kappa}{2h}(-u_{i-1}+u_{i+1})-GA\kappa\psi_i+\frac{EI}{h^2}(\psi_{i-1}-2\psi_i+\psi_{i+1})+\omega^2\rho I\psi_i-\tilde{K}^{\psi,u}_{i,j}u_j-\tilde{K}^{\psi,\psi}_{i,j}\psi_j=-\tilde{K}^{\psi,u}_{i,j}u^g_j-\tilde{K}^{\psi,\psi}_{i,j}\psi^g_j \quad (4.31)$$

$$\frac{EA}{h^2}(w_{i-1}-2w_i+w_{i+1})+\omega^2\rho A w_i-\tilde{K}^{w,w}_{i,j}w_j=-\tilde{K}^{w,w}_{i.j}w^g_j \tag{4.32}$$

with $i=1,...,n$ and $j=0,...,n+1$, $z_i=L_0$ representing the location of the tower top and $z_n=L$ that of the pile tip. This implies that two ghost nodes ($j=0$ and $j=n+1$) are used to solve the equations at the boundaries of the domain. The tildes over the global stiffness matrices in equations 4.30 - 4.32 indicate that these stiffness matrices are auxiliary matrices, incorporating the Trapezium rule for integration. In this case the Trapezium rule modifications are applied by multiplying the first and last columns of the original stiffness matrices by a factor $\frac{1}{2}$. Moreover, to include the ghost nodes a column of zeros is added to the left and right side of the matrices. To incorporate the boundary conditions (formulated in Eqs. 4.15 to 4.20) in the system of equations, these are rewritten into the following form:

$$GA\kappa\Big(\frac{-u_0+u_2}{2h}-\psi_1\Big)=-M_{RNA}\omega^2u_1, \qquad u_0=\frac{2h}{GA\kappa}M_{RNA}\omega^2u_1-2h\psi_1+u_2 \tag{4.33}$$

$$EI\Big(\frac{\psi_0+\psi_2}{2h}\Big)=J_{RNA}\omega^2\psi_1, \qquad \psi_0=-\frac{2h}{EI}J_{RNA}\omega^2\psi_1+\psi_2 \tag{4.34}$$

$$EA\Big(\frac{-w_0+w_2}{2h}\Big)=-M_{RNA}\omega^2w_1, \qquad w_0=\frac{2h}{EA}M_{RNA}\omega^2w_1+w_2 \tag{4.35}$$

$$GA\kappa\Big(\frac{-u_{n-1}+u_{n+1}}{2h}-\psi_n\Big)=0, \qquad u_{n+1}=2h\psi_n+u_{n-1} \tag{4.36}$$

$$EI\Big(\frac{-\psi_{n-1}+\psi_{n+1}}{2h}\Big)=0, \qquad \psi_{n+1}=\psi_{n-1} \tag{4.37}$$

$$EA\Big(\frac{-w_{n-1}+w_{n+1}}{2h}\Big)=0, \qquad w_{n+1}=w_{n-1} \tag{4.38}$$

These expressions need to be substituted into the equations 4.30 to 4.32 for $i=1$ and $i=n$, such that the ghost nodes ($j=0$ and $j=n+1$) can be eliminated. In this way a square matrix of $n\times n$ is obtained that can be inverted. By collecting the terms in 4.30 - 4.32 in a coefficient matrix **A** and a right hand side vector **b**, the solution vector **x** (containing $u$, $\psi$ and $w$) can be found by solving the linear algebraic equation $\mathbf{Ax}=\mathbf{b}$.

## 4.7. Summary

By making use of dynamic substructuring a modelling method is provided to obtain an effective 1D SSI model, that captures the soil impedance and seismic excitation by making use of 3D modelling. This method analyses the full soil-structure system by means of its components; the structure and the soil with excavation. By applying coupling procedures at the soil-pile interface the response of the full system can be determined.

The impedance of the soil is integrated into the 1D model by extracting Winkler foundation stiffness matrices using the non-local method of Versteijlen [30]. This is not only done for lateral and rotational motion of the pile, but also for the vertical motion. For the dynamic case, the soil stiffness matrices incorporate, besides inertial effects, also the material and geometric damping simulated in the 3D model, which makes them complex-valued and frequency dependent.

The seismic action is introduced into the 1D model by the ground displacements obtained in a separate substructuring step. In this step the soil subsystem - which incorporates an excavation at the location of the embedded pile - is subjected to the seismic bedrock excitation. The ground motion at the surface that forms the interface with the structure, is captured. In order to be compatible with the 1D model of the pile this is seismic ground motion is obtained as a function of merely one coordinate. By incorporating the excavation in the soil subsystem, the modelling approach accounts for the effect of wave diffraction in determining the effective seismic excitation of the structure.

In order to verify the effectiveness of the provided modelling approach, Chapter 5 will compare the results of the 1D model with those obtained by the full 3D soil-structure model.

# 5

# Validation

With the substructuring method of analysis introduced in Chapter 4, an approach is established to capture 3D soil-structure interaction effects into an effective one-dimensional model. The significant increase in computational speed associated with the translation from 3D to 1D is of great value for the design of offshore wind turbines. However, in order for the method to be effective, the identified 1D model should prove to adequately match the rigorous modelling results. For this reason, this chapter will present a comparison between the results obtained with the 3D and 1D modelling approaches in Section 5.1. In Section 5.2 the performance of the 1D model is discussed and the modelling limitations are identified.

## 5.1. Comparison with 3D model

Besides using the MATLAB based 3D FE model for extracting the soil impedance and the seismic ground motion, the model is also used for the three-dimensional target solution. In this section, the results of the 1D effective modelling approach are compared to the 3D modelling results. For this purpose, both models are used to determine the steady state response of the structure to seismic loads introduced by a uniform harmonic bedrock excitation. The accuracy of the solution is evaluated by making use of misfit functions. Depending on the aim of the analysis, the definition of the optimum might differ. For a specific type of analysis, an accurate match of the displacement and rotation at mudline is sufficient, while for the other a full match in bending moment for all depths might be preferred. In this work, the accuracy of the identified 1D model is assessed based on the response of the full embedded part of the pile. As the superstructure is not directly interacting with the soil, this part is not included. The misfit function considers the relative difference between the response of the 1D model and 3D model, in terms of the components; $u(z)$, $\psi(z)$, $w(z)$, $\frac{du}{dz}(z)$, $\frac{du}{dz}(z)$ and $\frac{du}{dz}(z)$, in the domain $z = (0, L)$.

$$
\begin{aligned}
C_{u,u',\psi,\psi',w,w'} = \frac{1}{6}\Big(C_u + C_{u'} + C_\psi + C_{\psi'} + C_w + C_{w'}\Big) = \\
\frac{\sum_{i=0}^{i=L}|u_{i,1D} - u_{i,3D}|}{6\sum_{i=o}^{i=L}|u_{i,3D}|} + \frac{\sum_{i=0}^{i=L}|u'_{i,1D} - u'_{i,3D}|}{6\sum_{i=0}^{i=L}|u'_{i,3D}|} + \frac{\sum_{i=0}^{i=L}|\psi_{i,1D} - \psi_{i,3D}|}{6\sum_{i=0}^{i=0}|\psi_{i,3D}|} + \\
\frac{\sum_{i=0}^{i=L}|\psi'_{i,1D} - \psi'_{i,3D}|}{6\sum_{i=0}^{i=0}|\psi'_{i,3D}|} + \frac{\sum_{i=0}^{i=L}|w_{i,1D} - w_{i,3D}|}{6\sum_{i=0}^{i=L}|w_{i,3D}|} + \frac{\sum_{i=0}^{i=L}|w'_{i,1D} - w'_{i,3D}|}{6\sum_{i=0}^{i=L}|w'_{i,3D}|}
\end{aligned}
\tag{5.1}
$$

Figure 5.1 to 5.4 display the complex-valued response of the 1D model and the 3D model for the two different soil profiles and excitation frequencies of 0.5 Hz and 2.0 Hz. The corresponding misfit values are presented alongside. These two frequencies are analyzed as they provide a good indication of the overall performance of the model in the frequency range relevant for seismic analysis of offshore wind turbines. The frequency $f = 0.5$ Hz is below the fundamental frequency of the soil-structure systems considered in this work, while $f = 2.0$ Hz is located above this frequency. Therefore, the response is stiffness-dominated for $f = 0.5$ Hz and more inertia-dominated for $f = 2.0$ Hz. Furthermore, the excitation frequency of $f = 0.5$ Hz is particularly interesting to analyze as it is located close to both the typical first and second bending mode of tower as well

as the first blade modes. The frequency of $f = 2.0$ Hz is considered as it located around the peak of typical seismic response spectra [8].

Figure 5.1 to 5.4 show a good match between the pile response obtained with the 1D model and the response of the 3D model. Especially, the fit of the real part of the complex-valued response is satisfactory. Although larger misfits are obtained for the imaginary part, which is related to the damping, also this part matches the 3D response relatively well. In Table 5.1 the misfit values for the four different cases are presented. The given values - representing the overall accuracy of the effective modelling method - are the averaged misfits in the frequency range between 0.1 and 6.0 Hz. This specific frequency range is considered throughout this thesis as the frequency range relevant for the seismic analysis of OWTs. This is based on the typical characteristics of tectonic earthquakes as well as the dynamic properties of offshore wind turbine structures. Existing research and practical experience in the field of seismic analysis of OWTs indicate that offshore wind structures are predominantly excited within this frequency range [10]. Note that Figure 5.1 to 5.4 gives the response and corresponding misfits of the imaginary and real parts of the response separately, while the absolute values are considered when determining the overall misfits ($C_{u,u',\psi,\psi',w,w'}$).

| Case | Soil profile | Soil inside MP | Overall accuracy |
|---|---|---|---|
| 1A | Homogeneous | Yes | 3.88 % |
| 1B | Homogeneous | No | 7.94 % |
| 2A | Heterogeneous | Yes | 2.68 % |
| 2B | Heterogeneous | No | 5.04 % |

Table 5.1: The accuracy of the 1D modelling results with respect to the target solution obtained with the 3D soil-structure model. The value is based on the overall misfit averaged over the frequency range between 0.1 and 6.0 Hz: $C_{u,u',\psi,\psi',w,w'}$ (0.1 − 6.0 Hz) × 100%.

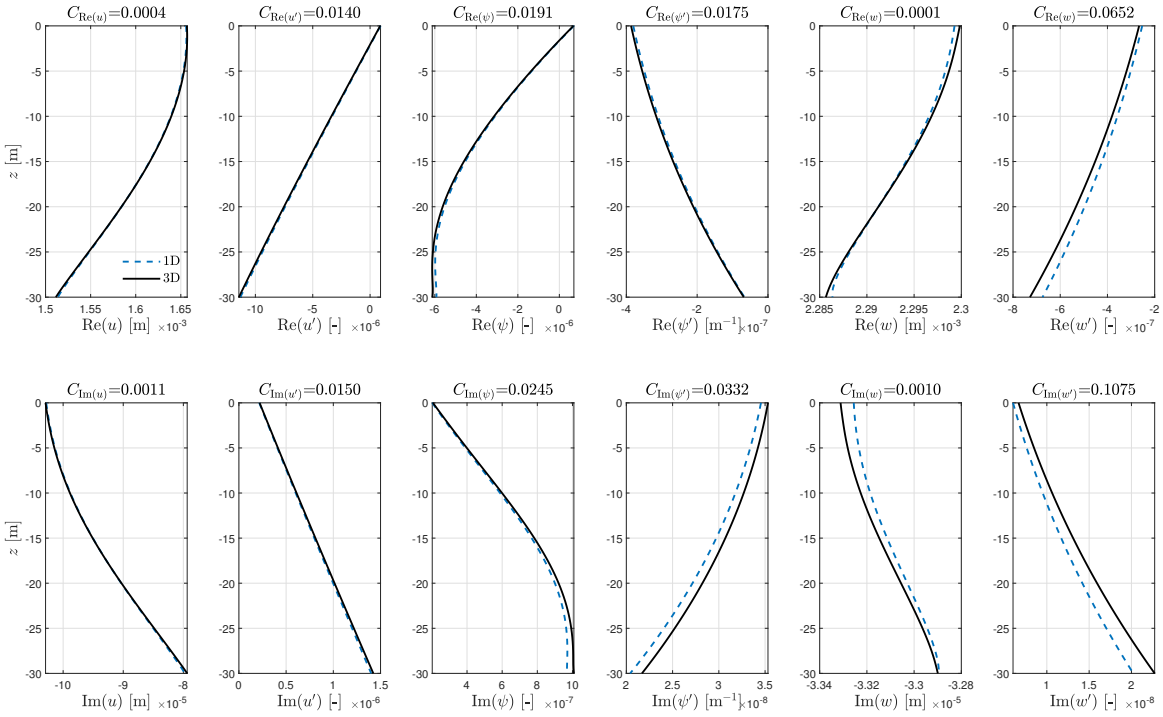


Figure 5.1: The fits between the complex-valued response of the 1D non-local model and the 3D model, for the homogeneous soil profile (Case 1A) and excitation frequencies of 0.5 Hz.

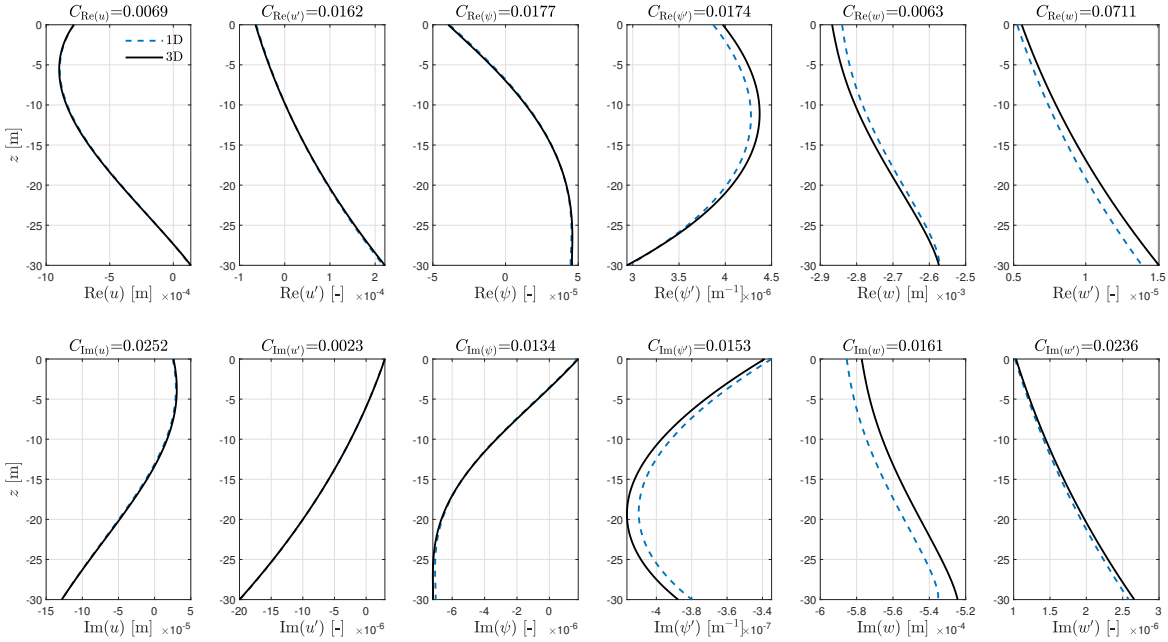


Figure 5.2: The fits between the complex-valued response of the 1D non-local model and the 3D model, for the homogeneous soil profile (Case 1A) and excitation frequencies of 2.0 Hz.

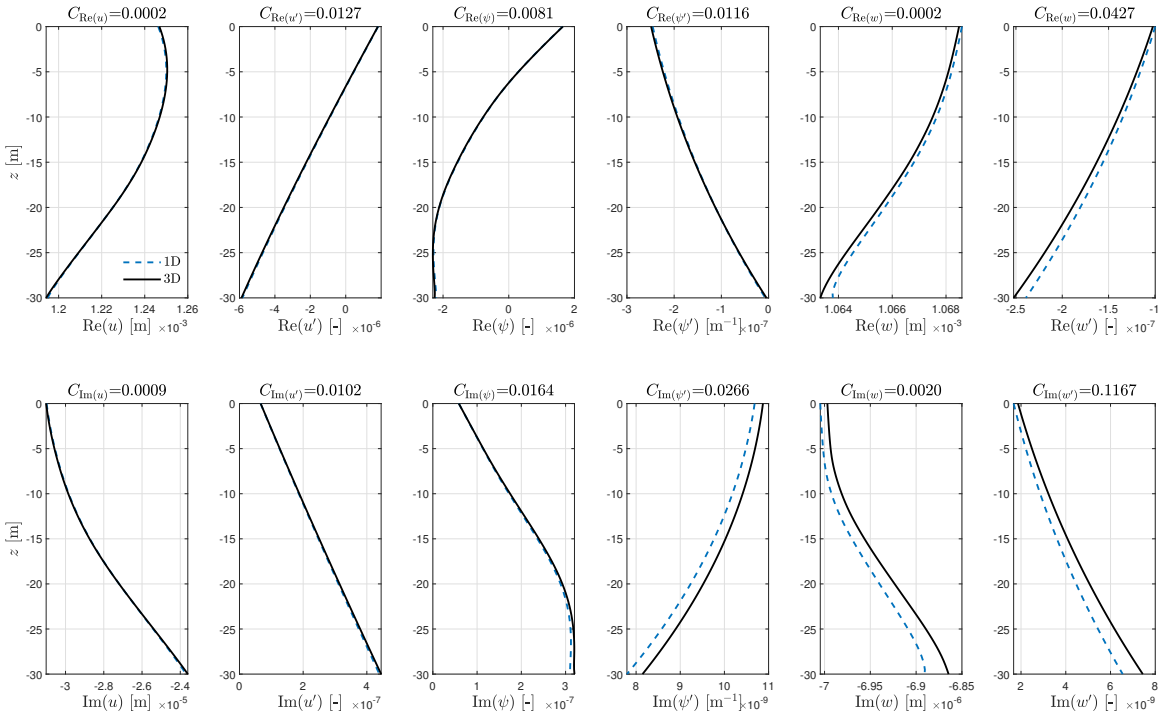


Figure 5.3: The fits between the complex-valued response of the 1D non-local model and the 3D model, for the heterogeneous soil profile (Case 2A) and excitation frequencies of 0.5 Hz.

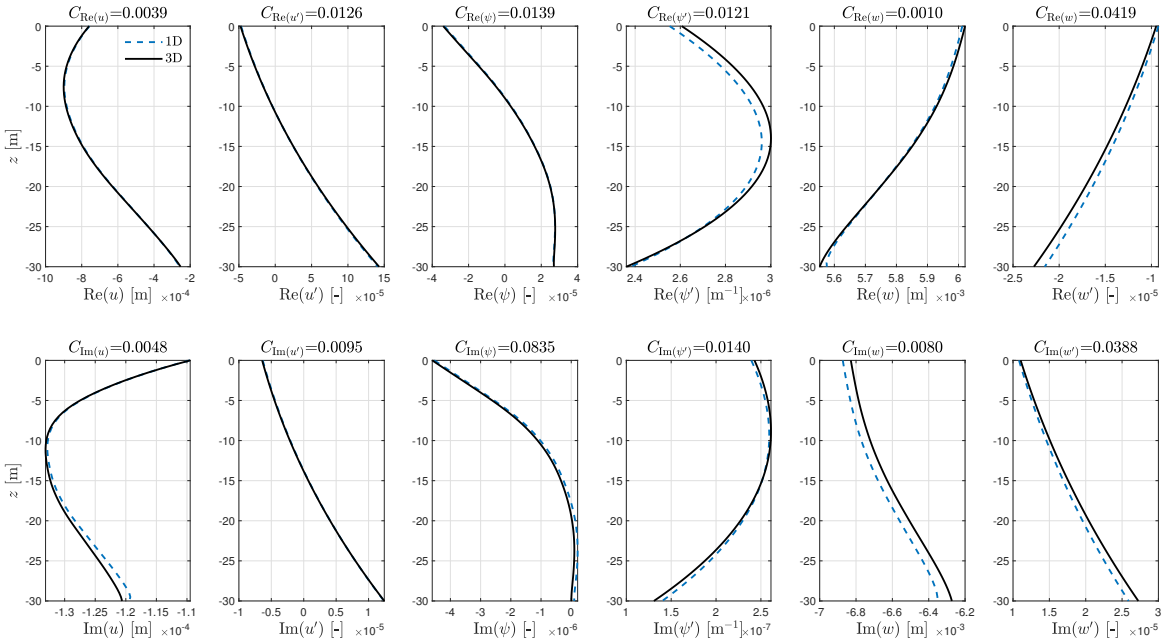


Figure 5.4: The fits between the complex-valued response of the 1D non-local model and the 3D model, for the heterogeneous soil profile (Case 2A) and excitation frequencies of 2.0 Hz.

## 5.2. Modelling limitations

The presented match between the 1D model and the 3D model are relatively good and within the accuracy limits that are acceptable in the seismic design procedure. Nevertheless, differences can be observed between the response of the 1D model and that obtained with the 3D soil-structure model. These differences predominantly originate due the applied assumptions to translate the three-dimensional problem into one dimension. Among others, this includes the different modelling methods of the pile; 1D Timoshenko beam versus the 3D solid elements. Relatively high misfits are identified for excitation frequencies corresponding to the resonance modes of the structure, this can be seen in Figure 5.5. These results indicate that the the difference in structural modelling may significantly contribute to the observed inaccuracy. To assess if these high misfits are related to the difference in structural modelling an analysis is performed that does not include a superstructure (tower and lumped RNA mass). Hence, for this specific case, the difference between the 1D model and 3D model is solely associated with the modelling of the soil-monopile system. In Figure 5.5 the difference in response between the 1D model and the 3D model is presented in terms of the misfit value $C_{u,u',\psi,\psi',w,w'}$ for both the situation with and without superstructure. The presented results confirm that the high misfit peaks are due to the difference in 1D versus 3D superstructure modelling and are not related to the soil impedance or seismic input.

Another possible cause of the misfit between 1D and 3D is related to the extraction of the 3D continuum soil reaction. The soil impedance matrices are determined based on beam-shaped (rigid ring) deformations, whereas the 3D soil-pile model allows for difference of the displacement along the circumference of the pile. Versteijlen [30] verified that the ovelisation of the 3D pile is higher for relatively soft soil conditions. This explains the higher misfit for Case 1 compared to Case 2, because the overall soil stiffness is lower for the homogeneous soil profile. A similar explanation can be provided for the difference between the cases with and without soil inside the monopile. The soil inside the foundation impedes the ovelisation of the pile. Thus, when removing this inner soil, larger differences of the displacement along the pile circumference will occur and the assumption of rigid ring deformations in extracting the 3D continuum soil reaction is less accurate.

Another assumption is made in determining the scattered ground motion required for the effective 1D modelling approach, by making use of the soil substructure. In determining the motion at the cavity surface for the cases with soil inside the monopile, the restriction is applied that the inner soil and outer soil are coupled

at each level of $z$. This introduces non-physical forces that result in an incorrect application of the substructuring approach, as the cavity surface is no longer a stress-free surface. This assumption causes additional inaccuracy in the translation from 3D to 1D. When no soil is included inside of the monopile (Case 1B and 2B), this restriction is not required and the motion at the outer cavity surface is simply averaged at each level of $z$ to obtain ground motion compatible with the 1D model. This approach however does not account for the differential motion along the circumference of the cavity. Again, the ovelisation - in this case of the cavity surface - is expected to be larger for relatively soft soil conditions.

Besides modelling uncertainties related to the behaviour of soil-structure system also the numerical approximations contribute to the deviation between 1D and 3D results. The mesh grid of the pile and soil domain is optimized based on a combination of modelling accuracy and computational efficiency. With a finer mesh the accuracy of the numerical approximation still improves. This is discussed in the mesh study of Appendix A. This predominantly affects the accuracy at higher frequencies as in this case the wavelength is shorter. This requires a finer mesh to have the same number of finite elements describing a full wavelength. For the discretization in the horizontal direction this is accounted for by decreasing the element width for higher frequencies. However, the vertical discretization is kept constant at 0.5 m because of computational limitations. Furthermore, even though Perfectly Matched Layers are incorporated, reflection of waves at the outer boundaries of the soil domain may still affect the modelling results.

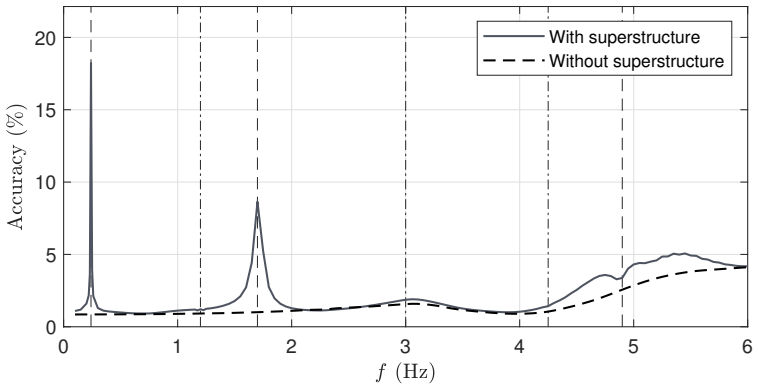


Figure 5.5: The accuracy with respect to the modelled 3D response for Case 2A, plotted over the frequency range of interest. The accuracy value is based on the overall misfit averaged over the frequency range between 0.1 and 6.0 Hz: $C_{u,u',\psi,\psi',w,w'}(0.1-6.0\text{ Hz}) \times 100\%$. A comparison is made for the case with and without superstructure to identify the influence of the difference in superstructure modelling. Pile resonances are indicate with (– – – -) and soil resonances with (· – · – ·).

# 6

# Application

Besides facilitating efficient seismic load simulations, the provided effective modelling approach can also be applied to obtain an improved understanding of the physical process of seismic soil-structure interaction. In this chapter the effective modelling method is used to analyze the influence of 3D continuum SSI effects on the dynamic response of OWTs, with the objective of identifying improvement opportunities in terms of modelling accuracy and efficiency. Based on these qualitative analyses, recommendations for the practical application of the effective modelling method will be presented.

One of the main advantages of the substructuring approach is that it allows for independent modelling of the different components. In this way, every modelling step can be optimized individually. In this chapter, the two soil-related components required to define the seismic soil-structure interaction problem are individually treated. In section 6.1, the effective seismic ground motion is addressed and a qualitative study is performed on wave propagation phenomena and their influence on the seismic loading of OWTs. In Section 6.2 the frequency dependent characteristics of the soil impedance is discussed. Lastly, Section 7.2 presents recommendations for the practical application of the non-local method for seismic load simulations in the design procedure of offshore wind turbine support structures.

## 6.1. Effective seismic excitation

The starting point of the seismic analysis using an effective Winkler-type model is determining the seismic ground motion to apply in the soil-structure model. This is a vital modelling step as inadequate consideration of the excitation load transferred to the foundation may results in significant under- or overestimation of the structural response. In this section, two important phenomena related to seismic wave propagation are discussed and their influence on the response of the structure is identified. First, the influence of the wave diffraction on the seismic excitation load is discussed in Section 6.1.1. In Section 6.1.2 the vertical wave passage effects are studied to analyze the influence of the varying ground motion along the embedded length of the monopile.

### 6.1.1. Wave diffraction

In conventional modelling procedures for seismic analyses, the ground motion used as input for the Beam-on-dynamic-Winkler-foundation model is determined based on a free-field ground response analysis. This is desirable because this reduces the complexity of the modelling process and, under certain assumptions, allows for using simple one-dimensional models to simulate the propagation of seismic waves through the soil deposit. As discussed in Section 4.2, the assumption behind using free-field ground motion is that the excitation loads due to diffraction of the incoming seismic waves can be neglected. Or formulated along the lines of the substructuring method established in Chapter 4; the presence of the pile cavity does not affect the earthquake induced motion of the soil subsystem.

As the response of the structure is of primary relevance, the effect of the different approaches to determine the effective seismic input is assessed based on the frequency response of the offshore wind turbine structure. For this purpose, the amplitude ratio between the uniform horizontal bedrock displacement and the tower

top displacement is presented in Figure 6.1, for Case 1A and 2A. The same is done for the bending moment at mudline level. The modelling results of the cases with soil inside of the tubular monopile section, do not indicate a significant difference in structural response between the two different 1D model. Both approaches capture the 3D soil-structure interaction relatively well, indicating that under the given circumstances the diffraction of seismic waves can be neglected.

The diffraction due to a disturbance in the soil medium is proportional to the dimensions of the obstacle causing the disturbance. If the dimensions of the irregularity - in this case the space occupied by the pile - would increase with respect to the wavelength, the diffraction would increase as well. For this reason, the space occupied by the pile is increased by assuming that the monopile is not filled with soil. Even though, the dimension of the pile itself are unchanged, this assumption leads to a larger disturbance of the free-field soil because of the larger excavation. Also for this case, the structural response to the horizontal bedrock excitation is analyzed based on the frequency response function of the tower top displacement and bending moment at mudline. This is presented in Figure 6.1.

The results of the 'empty' monopile-foundation, indicate that for this case the diffraction of the incident wave field does affect the seismic excitation load acting on the structure. By neglecting the influence of diffraction the response of the structure is overestimated. Moreover, the accuracy of the 1D non-local model using free-field ground motion as seismic input is lower compared to the 1D non-local model that accounts for wave diffraction by using the scattered ground motion as input. The misfits of the 1D pile response with respect to the modelled 3D response are presented in Table 6.1. Similar to Section 5.1, these values are based on the averaged overall misfits in the frequency range 0.1-6.0 Hz. The larger difference between the two 1D modelling approaches for high excitation frequencies, can be explained by the length of the seismic waves traveling through the system. Presuming that the wave medium remains unchanged, higher frequencies result in shorter wavelengths. As short waves with respect to the size of the disturbance experience more diffraction, a larger difference will be observed between the motion of the free-field soil and the disturbed soil body.

It has to be noted that in reality the monopile will never be completely free of soil inside the tubular section. This case is primarily considered to verify that the substructuring approach using the soil subsystem with excavation provides different and more accurate results with respect to the 3D target solution.

### 6.1.2. Vertical wave passage effects

An often-applied assumption in the seismic analysis of structures is that the seismic ground motion is uniform over the depth and can be represented by the motion at the ground surface. Due to this simplification, it is not required to determine the subsurface soil motion. By applying this approach, the fact that the ground motion induced by vertically propagating body waves varies over the depth, is not accounted for. To assess the influence of this assumption, the response of the structure is simulated by using the 'actual' non-uniform ground motion and by applying the simplified modelling approach that uses the ground surface motion along the full embedded pile length. In Figure 6.2, results are presented in terms of tower top displacements and bending moment at mudline, for both soil profiles.

It can be observed that the ground motion at the surface is not able to adequately describe the actual seismic excitation. This can be attributed to two effects. Firstly, the non-uniform ground motion along the pile introduces besides a translation also a rotation to the structure. As wind turbine structures are relatively tall structure, a small additional rotation at foundation level may result in significant differences in the response at tower top level. The second effect is related to the amplification of seismic ground motions towards the surface of the soil. In particular for the heterogeneous soil case, which is characterized by a relatively soft top layer, the superficial soil layers significantly amplify the ground motion amplitude. For this reason, the effective seismic excitation may be overestimated.

While the first effect generally results in an underestimation of the structural response, the second effect may cause overestimation. These opposing influences can be recognized in the frequency response of the heterogeneous soil case. Because the homogeneous soil profile does not have a soft superficial soil layer that amplifies the ground motion, the second effect does not noticeably influence the structural response for this case. Therefore, for Case 1A, an overestimation of the structural response is observed for the complete frequency range.

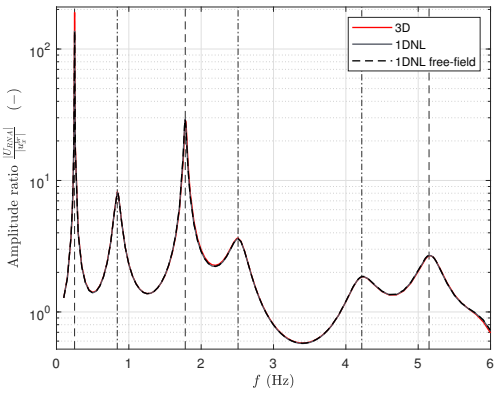


(a) Case 1A: $u_{RNA}$

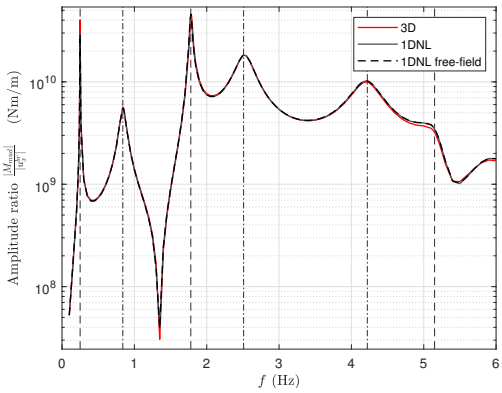


(b) Case 1A: $M_{mud}$

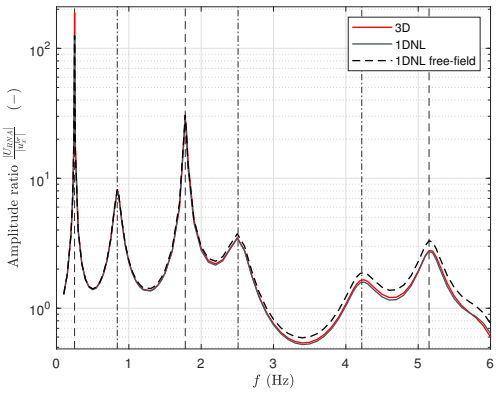


(c) Case 1B: $u_{RNA}$

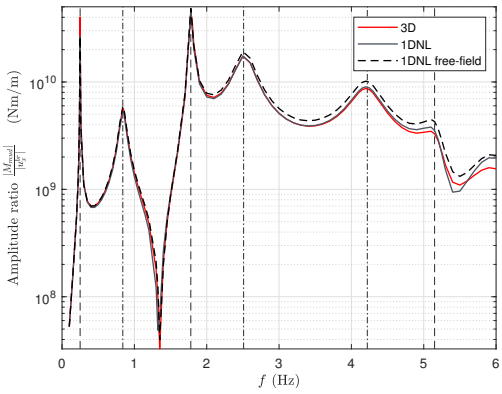


(d) Case 1B: $M_{mud}$

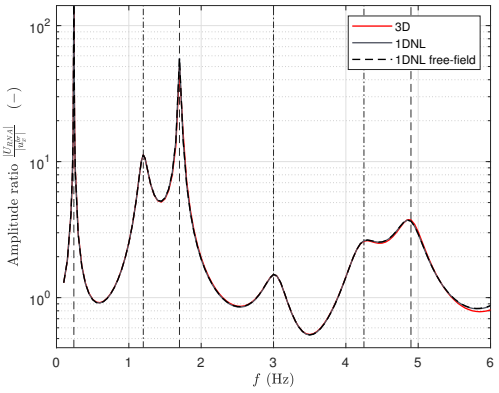


(e) Case 2A: $u_{RNA}$

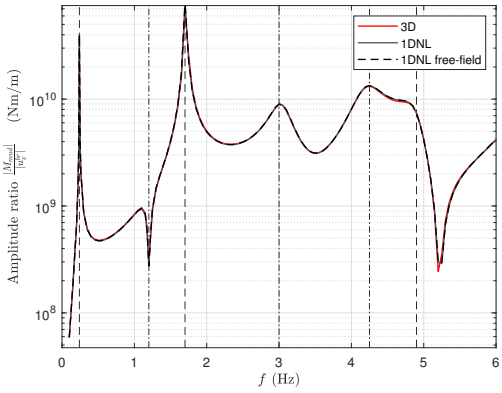


(f) Case 2A: $M_{mud}$

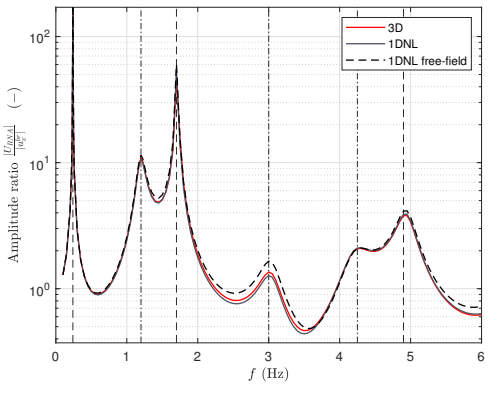


(g) Case 2B: $u_{RNA}$

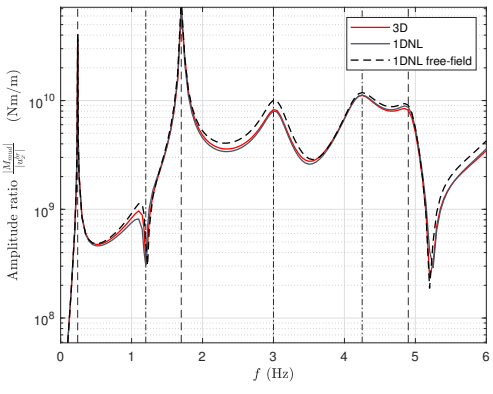


(h) Case 2B: $M_{mud}$

Figure 6.1: Frequency response functions of the tower top displacement and bending moment at mudline, normalized with respect to the amplitude of the horizontal bedrock displacement. A comparison is presented between the 3D model, the 1D non-local model using scattered ground motion (accounting for diffraction) and the 1D non-local model using free-field ground motion. Case 1A and 2A include soil inside the monopile and Case 1B and 2B are modelled without inner soil. Pile resonances are indicate with (– – – -) and soil resonances with (·–·–·).

| Case | Soil profile | Soil inside MP | Accuracy 1D NL | Accuracy 1D NL free-field |
|---|---|---|---|---|
| 1A | Homogeneous | Yes | 3.88 % | 4.15 % |
| 1B | Homogeneous | No | 7.94 % | 12.31 % |
| 2A | Heterogeneous | Yes | 2.68 % | 2.73 % |
| 2B | Heterogeneous | No | 5.04 % | 9.46 % |

Table 6.1: The accuracy of the 1D model response with respect to the 3D target solution. A comparison is made between the 1D model using free-field ground motion as input, and the 'exact' 1D model, using scattered ground motion. The value is based on the overall misfit averaged over the frequency range between 0.1 and 6.0 Hz: $C_{u,u',\psi,\psi',w,w'}(0.1-6.0\text{ Hz})\times 100\%$.

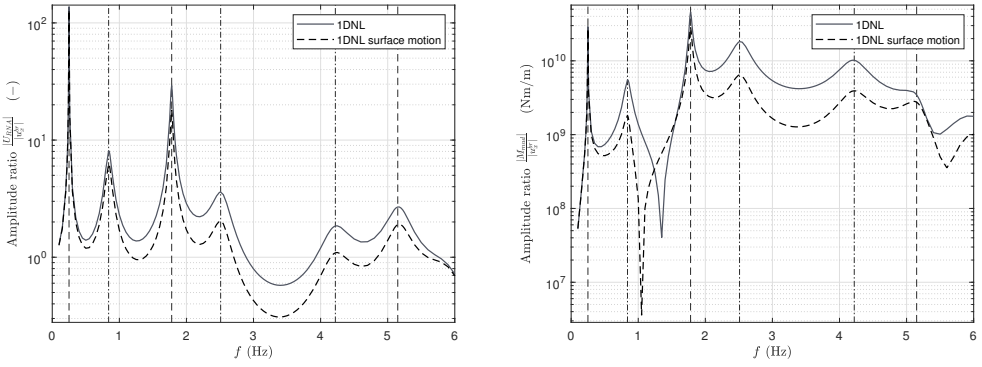


(a) Case 1A: $u_{RNA}$

(b) Case 1A: $M_{mud}$

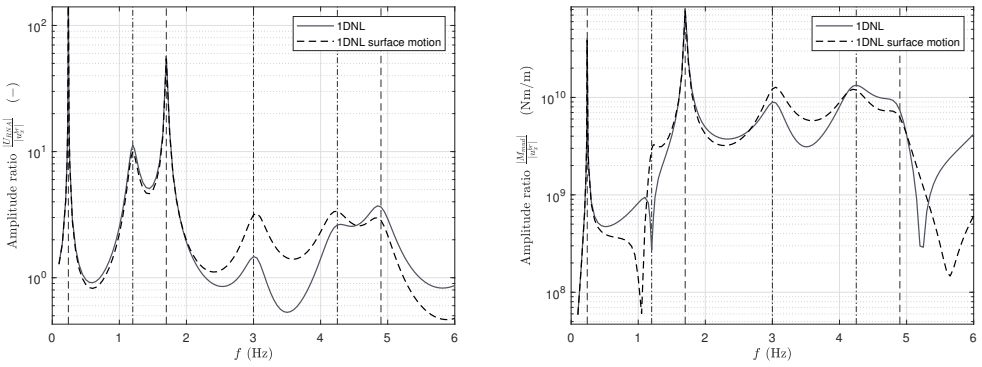


(c) Case 2A: $u_{RNA}$

(d) Case 2A: $M_{mud}$

Figure 6.2: Frequency response functions of the tower top displacement and bending moment at mudline, normalized with respect to the amplitude of the horizontal bedrock displacement. A comparison is presented between the 1D non-local model using the actual non-uniform ground motion along the monopile length and the 1D non-local model using the ground surface motion as input. Pile resonances are indicate with (− − −) and soil resonances with (·−·−·).

## 6.2. Soil impedance

In this section the characteristics of the soil impedance are evaluated in order to provide an improved physical understanding of the soil reaction towards monopile foundations during seismic loading. More specifically, the frequency dependent behaviour of the soil is analyzed and the influence of this behaviour on the offshore wind turbine's response is identified.

Owing to inertia forces of the soil and frequency dependent damping effects, the dynamic soil stiffness differs from the stiffness applicable for static conditions. To accurately account for this frequency dependent soil behaviour in dynamic SSI problems, the soil impedance must be determined for the full frequency range of interest. In this work the reaction of the three-dimensional stratified soil continuum is described using complex-valued, non-local soil stiffness matrices, as introduced in Section 4.4. The real part of these matrices represents the dynamic storage stiffness (in-phase stiffness and 180 degree out-of-phase inertia) of the

soil, while the imaginary part represents the damping. In order to identify the effects of the frequency dependent inertia forces of the soil, the real parts of the non-local soil stiffness matrices, $\mathbf{K}^{u,u}$, $\mathbf{K}^{\psi,\psi}$ and $\mathbf{K}^{w,w}$ are evaluated in the frequency range of interest. The same is done for the imaginary part. In order to asses the overall frequency dependent behaviour of the soil, the sum of the terms on the diagonal of the stiffness matrices is taken, as these are the terms dominating the global soil reaction:

$$k_{dsum}^{x,x}(\omega) = \sum_{i=1}^{n} \mathbf{K}_{ii}^{x,x}(\omega), \qquad x = u, \psi, w \tag{6.1}$$

These quantities are divided by the sum of the diagonal terms of the static soil stiffness matrices:

$$k_{dsum,0}^{x,x} = \sum_{i=1}^{n} \mathbf{K}_{ii}^{x,x}(\omega = 0), \qquad x = u, \psi, w \tag{6.2}$$

to obtain the ratios:

$$r_{Re}^{x,x}(\omega) = \frac{\Re\left(k_{dsum}^{x,x}(\omega)\right)}{k_{dsum,0}^{x,x}}, \qquad x = u, \psi, w \tag{6.3}$$

$$r_{Im}^{x,x}(\omega) = \frac{\Im\left(k_{dsum}^{x,x}(\omega)\right)}{k_{dsum,0}^{x,x}}, \qquad x = u, \psi, w \tag{6.4}$$

The ratios $r_{Re}^{x,x}(\omega)$ and $r_{Im}^{x,x}(\omega)$ - representing the real and imaginary part of the complex-valued dynamic soil stiffness normalized to the static soil stiffness - are plotted as a function of frequency in Figure 6.3. The figures display some characteristic behaviour of an elastic medium. Three frequency response ranges can be distinguished, which are defined by the frequency of excitation relative to the first natural frequency of the soil-pile system - also known as the cut-off frequency. The frequency ranges are:

- $\omega < \omega_{cut-off}$: The energy associated with the displacement of the pile is stored as elastic potential in the surrounding soil. There is no propagation of waves away from the structure and the damping purely consist of soil material damping. In this frequency range the ratio $r_{Im}^{x,x}(\omega)$ is equal to the loss factor. In this work this factor is assumed to be $\eta = 0.1$ (see Section 3.1).

- $\omega = \omega_{cut-off}$: The soil deposit is excited in its fundamental frequency, leading to standing waves in the in the vertical direction of the soil. The real part of the impedance shows a dip as the displacement resistance falls due to a large added soil mass.

- $\omega > \omega_{cut-off}$: The harmonic displacement of the pile leads to the generation of waves. These waves carry energy away from the system, which is felt as a damping force. Figure 6.3 clearly shows the increase of the imaginary part of the complex-valued soil stiffness for the range above the cut-off frequency.

The resonance dip does not only occur for the first natural frequency of the soil system, also at higher modes standing waves occur and the soil resistance drops. The ratio ($r_{Re}^{x,x}$) at resonance depends mainly on the material damping ratio of the soil and the impedance of the layer underlying the soil stratum. In this work the bedrock is assumed to be completely rigid, such that it reflects all downward propagating waves back into the system. This results in more pronounced resonance phenomena and a larger dip in the dynamic soil impedance compared to cases with a smaller impedance contrast between soil and bedrock. From Figure 6.3 it can be observed that the resonance of the soil stratum for vertical S-wave propagation predominantly affects the lateral soil reaction, while the resonance for vertical P-wave propagation mostly influences the vertical soil reaction.

The effect of the frequency dependent characteristics of the soil reaction on the structural response to earthquakes is studied as well. This is done by performing frequency response analyses of the monopile-supported offshore wind turbine using the effective 1D modelling approach. Two different cases are analyzed; one which accounts for the frequency dependent soil impedance and one case which assumes the soil stiffness to be frequency independent. In the first case, the soil stiffness matrices are separately extracted for each excitation frequency, while the second case uses soil stiffness matrices extracted at one frequency only. A frequency of

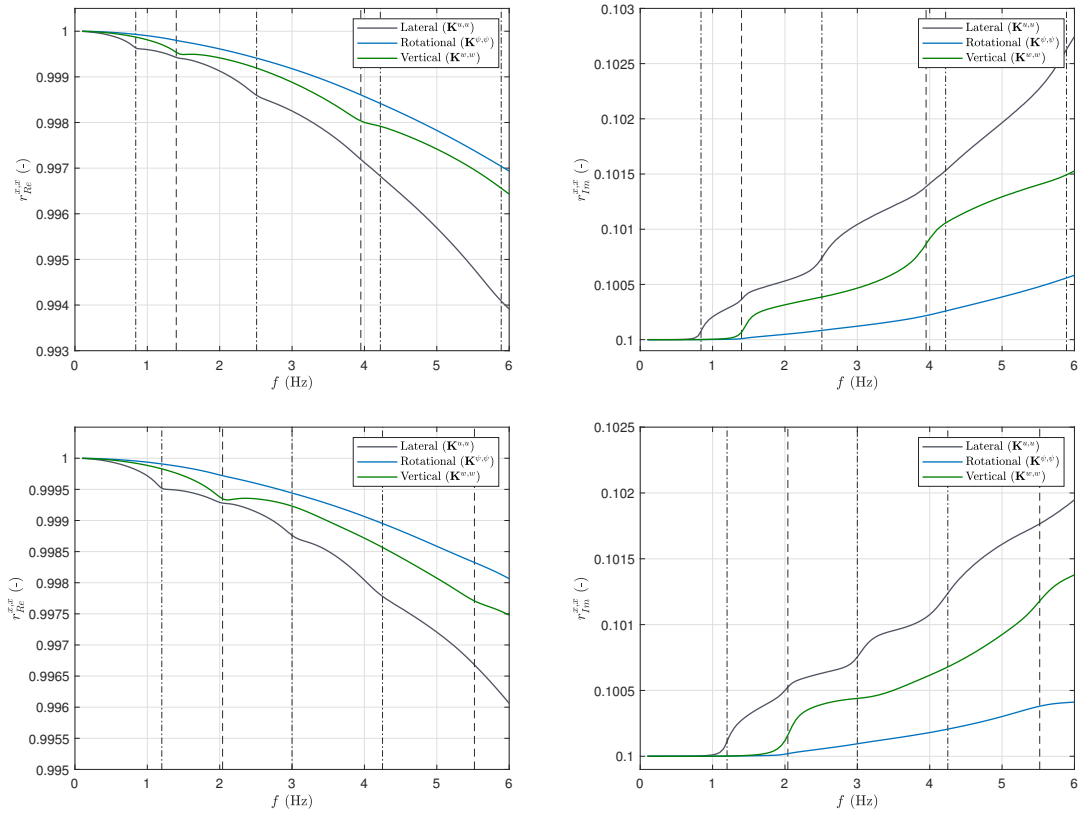


Figure 6.3: The real and imaginary part of the complex-valued dynamic soil stiffness as a function of the excitation frequency. The presented values are the sum of the diagonal terms of the soil stiffness matrices $\mathbf{K}^{u,u}$, $\mathbf{K}^{\psi,\psi}$ and $\mathbf{K}^{w,w}$, normalized to the corresponding static stiffness matrices. The resonance frequencies of the soil stratum for vertical S-wave propagation are indicated as (·−·−·) and for vertical P-wave propagation with (− − − -). The top figures correspond to the homogeneous (Case 2A) soil profile and the bottom figures to the heterogeneous (Case 2A).

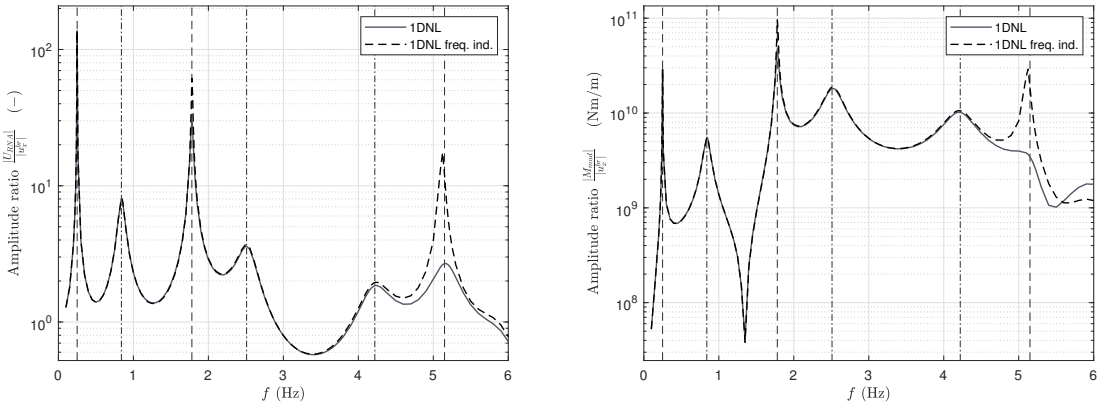


Figure 6.4: Frequency response functions of the tower top displacement and bending moment at mudline, normalized with respect to the amplitude of the horizontal bedrock displacement. A comparison is presented between the 1D non-local model using frequency dependent soil stiffness matrices and the 1D non-local model assuming frequency independent soil stiffness. Pile resonances are indicate with (− − − -) and soil resonances with (·−·−·).

$f$ = 0.2 Hz is used, as this is well below the first mode of the soil-pile system and therefore the stiffness matrices do not capture the effects of the resonance dips, radiation damping and soil inertia forces.

The frequency response functions of the tower top displacement and bending moment at mudline are displayed in Figure 6.4 for Case 1A; the homogeneous soil profile. These figures indicate that the response of the structure is overestimated for high excitation frequencies when not accounting for the frequency dependence of the soil impedance. At the second bending mode of the structure ($f$ = 1.78 Hz), the tower top displacement is overestimated with 93% and at the third mode ($f$ = 5.15 Hz) with 770 %. This is due to the geometric damping that is not included. Moreover, the frequency response functions show a small shift of the peaks corresponding to the resonant modes of the structure - especially, for the resonant peak at $f$ = 5.15 Hz. This can be attributed to the lower dynamic soil stiffness due to soil inertia forces.

## 6.3. Recommendations for practical application

The analyses performed in this chapter provide a better insight into the effects of soil-structure interaction on the offshore wind turbine's response to earthquakes. This can be used to identify the critical aspects in seismic analysis of offshore wind turbines and, moreover, it allows for identifying opportunities to improve the efficiency of the established 1D modelling approach. For each of the two soil-related components - the seismic ground excitation and the soil impedance - recommendations for the practical application are presented.

**Effective seismic excitation**

The provided effective modelling approach as presented in Chapter 4 includes a separate analysis step to determine the seismic ground motion; the ground response analysis. This motion introduces the earthquake excitation into the 1D model. The model used for the ground response analysis, must include an excavation in order to account for the effect of seismic wave diffraction. This requires the use of a 3D soil model, in which the case-specific geometry of the monopile foundation determines the dimensions of the excavation. This significantly increases the modelling complexity of this substructuring step, with respect to the conventionally applied free-field ground response analysis. Moreover, it makes it impossible to use the computationally efficient 1D wave propagation models to determine the seismic ground response.

As indicated by the analyses of Section 6.1.1, the difference between using free-field ground motion and the scattered ground motion, is insignificant - especially for the realistic case of the monopile foundation with soil inside the tubular section. The pile response obtained with the 1D model using free-field ground motion as input, matches the modelled 3D response equally well as the effective model that does account for diffraction. For this reason, it can be stated that for the practical application of the effective modelling approach, the modelling step to determine the seismic ground motion can be simplified by assuming free-field conditions.

The performed analyses are based on the assumption of a seismic wave field consisting of vertically propagating body waves. However, it is expected that the conclusions regarding the influence of diffraction do also apply for different seismic loading conditions - for example, for seismic action introduced by surface waves. Because wavelengths of surface waves are typically longer that those of shear waves [13], the influence of diffraction will not be larger for incoming surface waves.

**Soil impedance**

The method to identify an effective 1D model for seismic analysis, makes use of a 3D soil model to extract the 3D continuum soil reaction. By employing this approach continuum-related inertial effects, material damping and geometric damping of the soil are incorporated into the soil stiffness matrices. This makes the dynamic stiffness matrices, not only complex-valued but also frequency dependent. To account for this frequency dependence in an exact manner, the soil stiffness matrices must be extracted from the 3D model for the full frequency range of interest. This involves a great number of computationally demanding numerical calculations and therefore, a more efficient approach to account for the frequency dependent soil reaction is desirable.

To enable the identification of an efficient and accurate approach to account for the frequency dependent soil-structure interaction, insight is required in the SSI effect that cause this frequency dependency. These are the inertial forces of the soil and radiation damping effects. In Section 6.2, the characteristics of the dy-

namic soil reaction are analyzed. Based on this analysis it is observed that the participation of the geometric damping is limited with respect to the material damping of the soil, for the case studies analyzed in this work. Also the inertial effects of the soil only marginally affect the dynamic stiffness of the soil.

However, when looking at the response of the structure, the minor difference in dynamic soil stiffness, results in a noticeable difference of the structural response. In particular at frequencies corresponding to structural resonances (Figure 6.4). This is mostly related to the geometric damping effects - the effect of soil inertial forces is merely reflected by a small shift of the structural resonant frequencies. The added geometric damping considerably reduces the structural response at frequencies above the cutoff frequency of the soil. Therefore, it is beneficial to account for the effects of geometric damping in order to reduce the excitation of higher modes. However, it should be noted that one cannot always be sure that significant amount of energy will be dissipated in the form of radiation damping. When the soil deforms nonlinearly, the amount of energy that can be radiated away from the structure can be very limited as plastic waves cannot carry energy away in an efficient manner [2].

# 7

# Conclusion and recommendations

In this chapter a recapitulation is presented of the main findings of this research project. Moreover, as the work leaves behind interesting research opportunities for future efforts, some directions are listed for further work. First, in Section 7.1, the main conclusions are stated and in Section 7.2 recommendations for future research are presented.

## 7.1. Conclusion

The soil-structure interaction (SSI) of monopile foundations during earthquakes involves complicated load transferring mechanisms that can best be captured by an approach considering the soil as a three-dimensional continuum. However, 3D models are computationally too expensive for implementation in the design process of offshore wind turbine support structures. For this reason, the main objective of this master thesis is to *establish a method to identify an effective 1D model for seismic analysis of monopile-based offshore wind turbines that incorporates 3D soil-structure interaction.* Moreover, the aim is to use this effective method to assess the influence of 3D continuum soil-structure interaction effects on the offshore wind turbine's response to earthquakes. Based on this assessment, recommendations for the practical application of the effective modelling approach are provided.

In this study, a method is established that employs dynamic substructuring to capture the seismic excitation and 3D soil impedance in an effective 1D model. The method provides a substructure in the form of a Winkler foundation stiffness matrix along with the effective seismic ground motion over the embedded length of the pile, and integrates this in a 1D beam model. To obtain the foundation stiffness matrix, the non-local method of Versteijlen [30] is applied. This method directly extracts the global soil reactions from a 3D model, yielding an *exact* representation of the 3D soil impedance. The effective seismic ground motion is determined with the same 3D model of the soil subsystem. It is proven theoretically that the established modelling approach accounts for the full wave field, consisting of a free-field, diffracted and radiated component.

The effective 1D model identified by the substructuring approach was shown to closely match the response of a full 3D soil-structure model - for both horizontal and vertical earthquake motion. The small difference between the 1D and 3D modelling results are related to numerical errors and assumptions made to translate the 3D soil-structure interaction problem into 1D. The latter includes the different models used for the pile (1D beam versus 3D solid elements) and assumptions required to extract the 3D soil impedance and effective seismic ground motion as a function of one coordinate only. For the soil-structure characteristics and seismic environment considered in this work, the modelled structural response is however not significantly affected by these assumptions. Hence, it is verified that the developed modelling approach effectively captures the 3D soil-structure interaction during seismic loading.

Following the validation of the effective modelling method, the identified 1D model is employed to perform frequency domain analyses. Based on these analyses, the influence of 3D continuum soil-structure interaction effects on the structural response to earthquakes is assessed. This has led to two main conclusions.

First of all, it is concluded that the diffracted component of the seismic wave field does not significantly affect the earthquake excitation load acting on the monopile foundation. This is verified for a seismic wave field consisting of vertically propagating body waves. For these often assumed loading conditions, it is therefore possible to use free-field ground motion to introduce the seismic action in a Winkler-type model.

Secondly, by assessing the frequency dependent characteristics of the soil impedance and its effect on the offshore wind turbine's response, it is concluded that the soil-structure interaction during earthquakes should be considered as frequency dependent. This is required in order to account for inertial effects and geometric damping of the soil. The former results in a slight reduction of the dynamic stiffness of the soil, while the latter is reflected by an increased amount of energy dissipation for excitation frequencies above the first resonance of the soil-pile system. As the geometric damping results in a reduced motion of the structure, neglecting this additional damping component results in a conservative estimation of the structural response to seismic loading.

To recapitulate, this thesis provided a method to identify an effective soil-structure interaction model for seismic analysis of monopile-supported offshore wind turbines, that combines the computational speed of a 1D model with the accuracy of a 3D model. Moreover, recommendations for the practical application of this method are provided based on a qualitative assessment of continuum-related SSI effects on the structural response to earthquakes.

## 7.2. Recommendations

Based on the performed research in the current thesis, directions for further research are identified:

- The stress-strain relationship of soils is nonlinear. Nevertheless, the current work assumes the soil behaviour to be linear elastic. This is an often applied assumption for the initial, small-strain soil response. However, in regions with high seismicity and soft to medium soil conditions, one would expect a high degree of soil nonlinearity. In order to account for this within the presented effective modelling approach, the soil behaviour must be linearized. For this reason, it must be evaluated if a satisfactory approximation of the true non-linear soil behaviour can be obtained by applying this linearized modelling approach. This linearization can performed by making use of an iterative procedure to estimate the expected strain levels in the soil and in this way determine a secant soil stiffness. Fundamentally, this is not correct but for design purposes this approach could prove to be effective.
- The current method can also be extended to directly incorporate strain-dependent soil behaviour. The two soil-related substructuring steps - the ground response analysis and the extraction of the soil impedance - can each be performed using a nonlinear approach. For the ground motion this can straightforwardly be done by using a suitable nonlinear ground response model. For extracting the dynamic soil stiffness from a 3D soil model this is however more complicated. Extending the non-local effective stiffness method to incorporate soil nonlinearity is a topic of ongoing research. It should however be noted that the presented method is based on the principle of superposition, which is only exact for linear formulations. Therefore, in order to extend the current method to include nonlinear soil behaviour, it has to be investigated if the superposition of the free-field ground response and the SSI response still provides an accurate representation of the total motion of the system.
- Before applying the current method in the foreseen time-domain load simulations, a more extensive assessment of the frequency dependent characteristics of the soil-structure interaction must be performed. In particular the influence of the location and properties of the bedrock must be evaluated as this can significantly affect the dynamic characteristics of the soil deposit. Moreover, the effect of a lower soil material damping must be assessed as this could lead to more pronounced resonant dips in the dynamic stiffness. For capturing the frequency dependent SSI in a time domain model, it can be evaluated if an equivalent added soil mass and frequency-dependent dashpots can be found, that mimics the inertial and geometric damping effects of the soil.
- Besides analyzing seismic wave fields consisting of vertically propagating body waves, the method can also be applied for surface waves. For this purpose a suitable modelling method must be provided to determine the ground motion as induced by these surface waves. Moreover, it would be interesting to verify if also for this type of wave, the diffraction can be neglected and therefore free-field ground motion can be applied.

# A

# Mesh study

A mesh study is performed to determine a suitable discretization of the MATLAB based FE model to numerically approximate the continuous physical problem. This involves determining a mesh grid in the vertical direction and in the radial direction. In the radial direction, a lower accuracy is allowed towards the outer boundaries of the domain, as the domain in the vicinity of the monopile predominantly affects the structural response. Therefore, the element size gradually increases for an increasing radial distance from the central axis. In the vertical direction of the domain, accurate modelling is equally important along the depth and, therefore, a constant vertical spacing of the FE nodes is applied. Three different element heights are considered; 1.0 m, 0.5 m and 0.25 m.

For the radial discretization, also three options are considered. In the domain around the pile, the three considered options all use an element width equal to the pile thickness. From the outer boundary of pile, the element width starts to increase gradually with a ratio of 1.02 between every consecutive element. A maximum horizontal spacing, $dxMax$, is used to limit the maximum element dimensions. This $dxMax$ is related to the smallest wavelength present in the system:

$$dxMax = \frac{\lambda}{r_{dxMax}} \tag{A.1}$$

The ratio $r_{dxMax}$ is varied between 6 and 10 as is generally recommended in literature [37]. The five mesh grid options are presented in Table A.1. The performance of the different meshes is judged based on one control parameter; the absolute value of the pile displacement at mudline, $|u_{x,mud}|$. The case study used for the mesh evaluation is based on the homogeneous soil profile. For simplicity, no superstructure is modelled. It is verified that including a superstructure would not influence this comparative study. When smaller elements are used (a finer mesh), more accurate results are expected. For this reason, Figure A.1 displays results for the control parameter normalized to the result obtained with the finest mesh ($h$ = 0.25 m, $r_{dxMax}$ = 8). In this way, the relative difference between the different meshes is clearly visualized.

Based on the mesh study it can be concluded that changing the factor $r_{dxMax}$ between 6 and 10, does not affect the numerical results. Therefore the mesh used in this work will adopt $r_{dxMax}$ = 6. The different element heights $h$, do however significantly affect the results. For the mesh with $h$ = 1.0 m, the control parameter shows a deviation of 2 to 12% with respect to the target results obtain with the finest mesh (mesh option 5). For $h$ = 0.5 m this is a deviation between 0.5 and 4%. In general, the differences increase with higher frequencies. This can be explained by the fact that higher frequency excitation results in shorter wavelengths and therefore a finer mesh is required to describe a full wave with the same amount of elements. The difference in computational efficiency between a mesh with $h$ = 0.5 m and a mesh with $h$ = 0.25 m is very large and does not outweigh the increase in accuracy. Therefore, this work will employ **mesh option 4**: $h$ = 0.5 m and $r_{dxMax}$ = 6.

| Mesh option | dz | $r_{dxMax}$ |
|---|---|---|
| 1 | 1.0 m | 8 |
| 2 | 0.5 m | 10 |
| 3 | 0.5 m | 8 |
| 4 | 0.5 m | 6 |
| 5 | 0.25 m | 8 |

Table A.1: The different mesh grids evaluated in this study. The meshes differ in element height and maximum element width. The minimum element width is equal to the pile thickness.

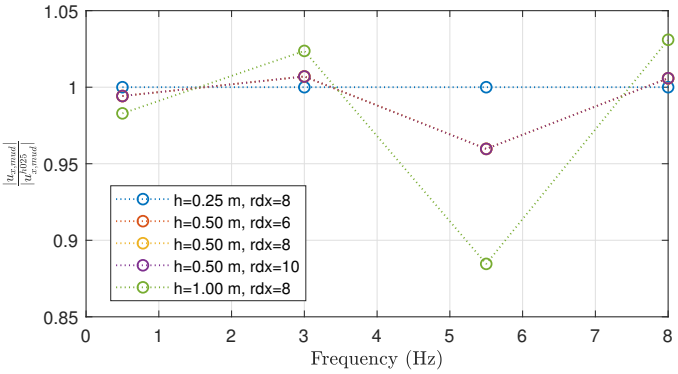


Figure A.1: The results of the mesh study in terms of the control parameter, $|u_{x,mud}|$. Which is the absolute value of the pile displacement at mudline. The plotted value is normalized with respect to the target solution obtained with the finest mesh grid.

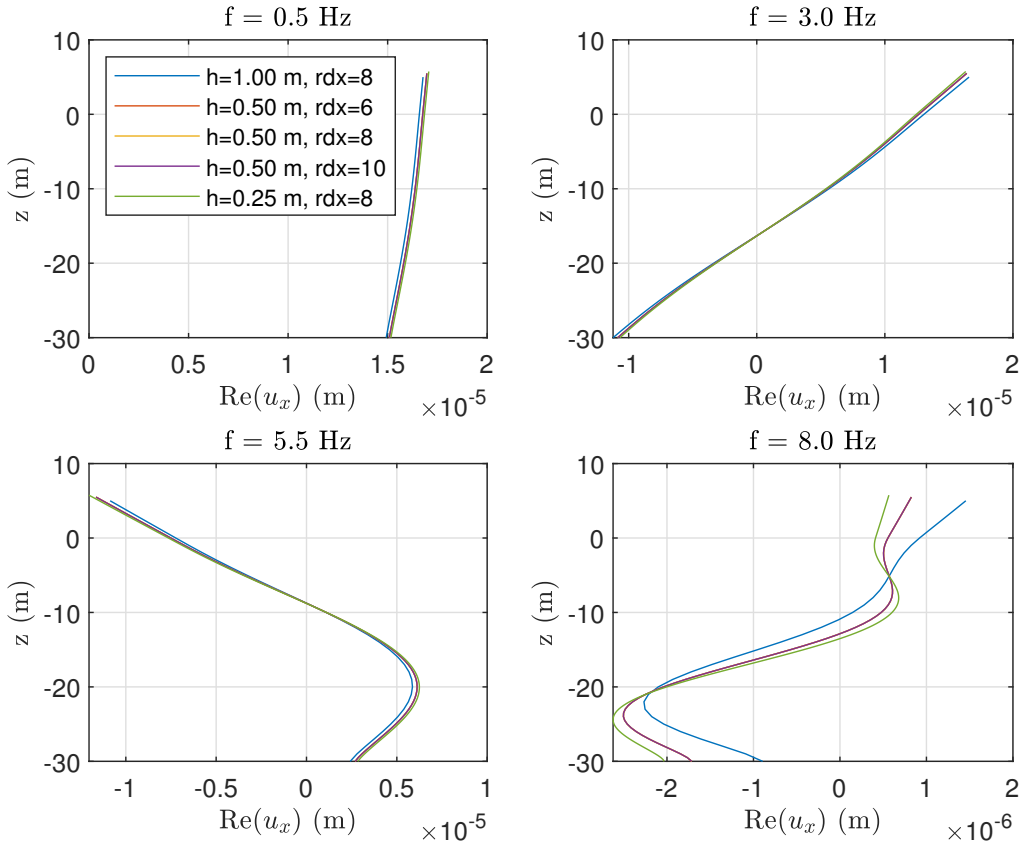


Figure A.2: The real part of the pile displacement (Re($u_x(z)$)) is plotted as an additional indication of the mesh performance.

# B

# Wave forces on a body

In Chapter 4, Section 4.1, the substructuring method of analysis is introduced to determine the forces acting on the structure due to seismic action and soil-structure interaction. This method is analogous with an often applied approach to determine forces arising from potential flow theory used in the field of hydrodynamics. As this resemblance is not directly apparent, this appendix will elaborate on the analogy between the two approaches. To do this we start from the equation identified in Section 4.1, which defines the forces on the structure. Next, we show that these are the same forces as encountered in hydrodynamics. The equation presented in section 4.1 that describes the forces acting from the soil towards the structure is defined as:

$$\mathbf{p}_f^t = \mathbf{G}_{ff}\left(\mathbf{u}_f^{g,e} - \mathbf{u}_f^t\right) \tag{B.1}$$

To clearly separate the two components, this equation is rewritten to:

$$\mathbf{p}_f^t = \mathbf{p}_f^I + \mathbf{p}_f^{II} \tag{B.2}$$

where $\mathbf{p}_f^I$ and $\mathbf{p}_f^{II}$ are defined as:

$$\mathbf{p}_f^I = \mathbf{G}_{ff}\,\mathbf{u}_f^{g,e} \tag{B.3}$$

$$\mathbf{p}_f^{II} = -\mathbf{G}_{ff}\,\mathbf{u}_f^t \tag{B.4}$$

In these equations, the following notations are used:

- $\mathbf{G}_{ff}$ is the matrix describing the dynamic stiffness of the soil body with excavation, for the nodes on the interface between soil and structure (denoted with subscript $f$).
- $\mathbf{u}_f^{g,e}$ contains the displacement amplitudes of the soil subsystem due to the seismic loading. In this loading state the surface of the soil system satisfies stress-free boundary conditions.
- $\mathbf{u}_f^t$ describes the total displacement of the structure at the soil-structure interface. These displacements are the same for the nodes $f$ positioned at the soil body.

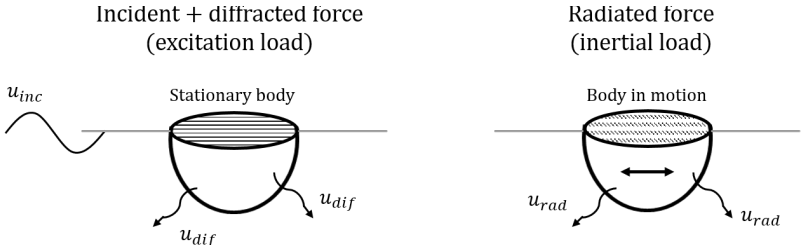


Figure B.1: A visualization of the loading states used in hydrodynamics to decompose the wave forces acting on a body.

**Decomposition of wave forces acting on a body**
The approach applied in the field of hydrodynamics, to determine wave forces acting on a body, separates the forces into three components [21]:

1. The force due to the incident wave field, $F_I$ (the Froude-Krylov force). This load is introduced by the pressure field generated by the free-field waves. In this situation the medium does not include a geometrical irregularity due to a structure or 'excavation'. This force does however include the effects of wave reflection of the free surface.
2. Diffraction or scattering force ($F_D$), which originate because the wave field near the body is affected even if the body is stationary (so that no-flux B.C. is satisfied).
3. Radiation force ($F_R$), which originates from to the total motion of the body in the absence of an incident wave field.

The combination of the first two components is generally referred to as the excitation load and the last component as the inertial load. The physical meaning of these components is visualized in Figure B.1.

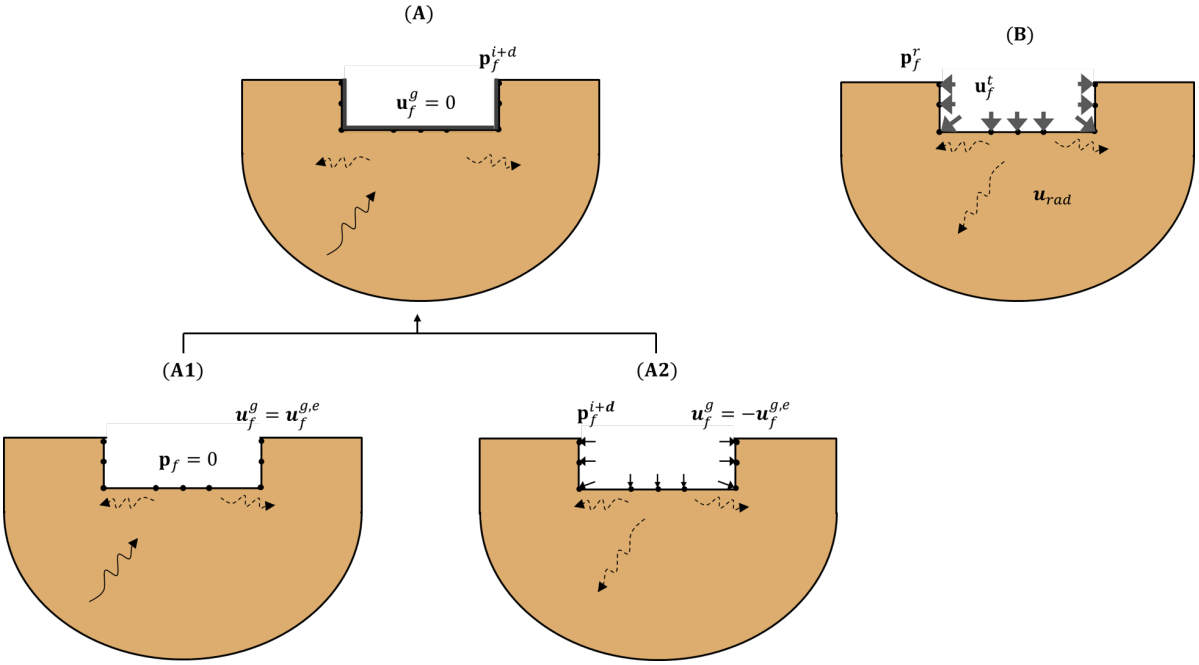


Figure B.2: The two loading states of the soil body with excavation to decompose the seismic soil-structure interaction forces. Loading state A captures the incident and diffracted fields, while loading state B includes the radiated field.

**Analogy between hydrodynamic and earthquake approach**
For the seismic SSI case considered in this work the same components can be identified. The component $\mathbf{p}_f^{II}$ describes the interaction forces developed due to the total structural motion in the absence of an incident wave field (see Figure B.2, component B). This corresponds to the third component of the hydrodynamic wave force decomposition (the inertial load). In this work these forces are referred to as the radiation forces and the corresponding wave field is called the radiated field ($u_{rad}$).

The physical explanation of component $\mathbf{p}_f^{II}$ is less straightforward. Even though it may not be directly obvious, these forces correspond to the field generated by the incident and diffracted waves. This can be proven by making use of superposition. The left loading state of Figure B.1 - representing the stationary structure subjected to the incoming seismic waves - can be decomposed into two components, as depicted in Figure B.2. In the first loading state, the complete surface is free of stress and the system is subjected to the incoming waves (component A1). The motion observed at the interface nodes ($f$) due to this loading state is by definition equal to $\mathbf{u}_f^{g,e}$.

The second component (A2 in Figure B.2) is generated by forces acting at the interface nodes:

$$\mathbf{p}_f^{g,inc+dif} = -\mathbf{G}_{ff}\mathbf{u}_f^{g,e} \tag{B.5}$$

These impose displacements such that the superposition of the two components (A1 and A2) satisfies the zero displacement conditions at nodes $f$:

$$\mathbf{u}_f^{g,inc+dif} = \mathbf{u}_f^{g,e} - \mathbf{G}_{ff}^{-1}\mathbf{p}_f^{g,inc+dif} = 0 \tag{B.6}$$

By making use of Equation B.3 it can be proven that the first component of the interaction forces acting on the structure, $\mathbf{p}_f^I$, indeed captures the incident and diffracted forces:

$$\mathbf{p}_f^I = \mathbf{G}_{ff}\mathbf{u}_f^{g,e} = \mathbf{p}_f^{g,inc+dif} \tag{B.7}$$

# C

# Numerical approximation of equations of motion

The differential equations describing the one-dimensional model of a beam on a non-local Winkler foundation are numerically solved using Euler's central finite difference scheme [5]. To verify the accuracy of this numerical approximation a sanity check is performed in this appendix. To satisfy equilibrium conditions the sum of the lateral forces, bending moments and vertical forces should be zero. However, as the obtained solution is a numerical approximation, a small error will appear. In this appendix it is evaluated if this error is sufficiently small compared to the individual force components.

By applying the central finite difference method the equations of motion can be formulated using Einstein summation convention, as presented in equations Eqs. 4.30 - 4.32. By collecting the terms in Eqs. 4.30 - 4.32 in a coefficient matrix **A** and a right hand side vector **b**, the solution vector **x** (containing $u$, $\psi$ and $w$) can be found by solving the linear algebraic equation $\mathbf{Ax} = \mathbf{b}$. By implementing the obtained nodal displacement amplitudes ($u$, $\psi$ and $w$) back into the equations of motion it can be verified if the equilibrium conditions are satisfied, i.e. if the sum of forces approaches zero. To evaluate this, the remaining horizontal force ($R_{f_x}$), bending moment ($R_m$) and vertical force ($R_{f_z}$), is determined and divided by the magnitude of the internal beam forces:

$$e_{f_x}(\omega, z) = \frac{R_{f_x}}{F_x^{in}} \tag{C.1}$$

$$e_m(\omega, z) = \frac{R_m}{F_m^{in}} \tag{C.2}$$

$$e_{f_z}(\omega, z) = \frac{R_{f_z}}{F_z^{in}} \tag{C.3}$$

with:

$$F_x^{in} = GA\kappa\left(\frac{d^2u(z)}{dz^2} - \frac{d\psi(z)}{dz}\right) \tag{C.4}$$

$$F_m^{in} = GA\kappa\left(\frac{du(z)}{dz} - \psi(z)\right) + EI\frac{d^2\psi(z)}{dz^2} \tag{C.5}$$

$$F_z^{in} = EA\frac{d^2w(z)}{dz^2} \tag{C.6}$$

The values of $e_{f_x}$, $e_m$ and $e_{f_z}$ provide an indication of the relative error. This error is plotted in Figure C.1 and C.2, for Case 1A and an excitation frequency of 2.0 Hz and 5.0 Hz. From these figure we can conclude that the errors are relatively small and the governing equations of the 1D model are accurately solved.

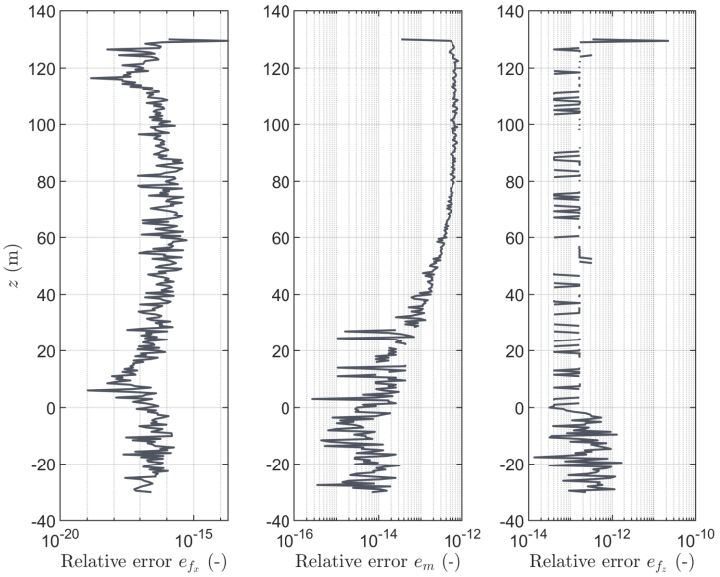


Figure C.1: The error in the numerical approximation for Case 1A and excitation frequency $f$ = 2.0 Hz

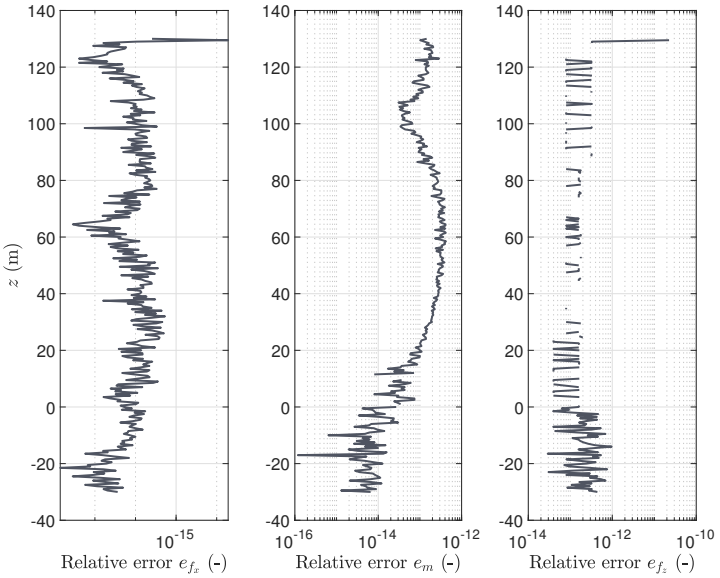


Figure C.2: The error in the numerical approximation for Case 1A and excitation frequency $f$ = 5.0 Hz

# Bibliography


[1] Natale Alati, Giuseppe Failla, and Felice Arena. Seismic analysis of offshore wind turbines on bottom-fixed support structures. *Philosophical Transactions of the Royal Society A: Mathematical, Physical and Engineering Sciences*, 373(2035):20140086, 2015.

[2] A.Tsouvalas. *CIE5260: Structural Response to Earthquakes*. TU Delft, 2018.

[3] Jean-Pierre Berenger. A perfectly matched layer for the absorption of electromagnetic waves. *Journal of computational physics*, 114(2):185–200, 1994.

[4] Fuquan Chen, Yujian Lin, Yizhi Dong, and Dayong Li. Numerical investigations of soil plugging effect inside large-diameter, open-ended wind turbine monopiles driven by vibratory hammers. *Marine Georesources & Geotechnology*, pages 1–14, 2019.

[5] Germund Dahlquist and Ake Bjorck. *Numerical Methods in Scientific Computing: Volume 1*, volume 103. Siam, 2008.

[6] Raffaele De Risi, Subhamoy Bhattacharya, and Katsuichiro Goda. Seismic performance assessment of monopile-supported offshore wind turbines using unscaled natural earthquake records. *Soil Dynamics and Earthquake Engineering*, 109:154–172, 2018.

[7] Det Norske Veritas DNV. Dnv-os-j101 offshore standard: Design of offshore wind turbine structures. *DNV AS, Høvik, Norway*, 2014.

[8] Amr S Elnashai and Luigi Di Sarno. *Fundamentals of earthquake engineering*. Wiley Online Library, 2008.

[9] Amir Reza Ghaemmaghami, Oya Mercan, and Reza Kianoush. Seismic soil–structure interaction analysis of wind turbines in frequency domain. *Wind Energy*, 20(1):125–142, 2017.

[10] Maria Luisa Rosales Gonzalez. *Seismic Analysis on Monopile Based Offshore Wind Turbines Including Aero-elasticity and Soil-Structure Interaction*. TU Delft, 2016.

[11] Ma Hongwang. Seismic analysis for wind turbines including soil-structure interaction combining vertical and horizontal earthquake. In *15th World Conference on Earthquake Engineering, Lisbon, Portugal*, 2012.

[12] T Ishihara and MW Sarwar. Numerical and theoretical study on seismic response of wind turbines. In *European wind energy conference and exhibition*, pages 1–5, 2008.

[13] Junbo Jia. *Modern earthquake engineering: Offshore and land-based structures*. Springer, 2016.

[14] Evangelos I Katsanos, Sebastian Thöns, and Christos T Georgakis. Wind turbines and seismic hazard: a state-of-the-art review. *Wind Energy*, 19(11):2113–2133, 2016.

[15] Eduardo Kausel and Joao Manuel de Oliveira Barbosa. Pmls: A direct approach. *International journal for numerical methods in engineering*, 90(3):343–352, 2012.

[16] Amir M Kaynia. Seismic considerations in design of offshore wind turbines. *Soil Dynamics and Earthquake Engineering*, 2018.

[17] Remi A Kjørlaug and Amir M Kaynia. Vertical earthquake response of megawatt-sized wind turbine with soil-structure interaction effects. *Earthquake Engineering & Structural Dynamics*, 44(13):2341–2358, 2015.

[18] Remi André Kjørlaug, Amir M Kaynia, and Ahmed Elgamal. Seismic response of wind turbines due to earthquake and wind loading. In *Proceedings of the 9th international conference on structural dynamics, EURODYN*, 2014.

[19] Germanischer Lloyd and Germany Hamburg. Guideline for the certification of offshore wind turbines, 2005.

[20] Hudson Matlock. Correlations for design of laterally loaded piles in soft clay. *Offshore technology in civil engineering's hall of fame papers from the early years*, pages 77–94, 1970.

[21] John Nicholas Newman. *Marine hydrodynamics*. MIT press, 2018.

[22] Japan Society of Civil Engineers. *Guidelines for design of wind turbine support structures and foundations*. JSCE, 2010.

[23] Michael W O'Neill and Jack M Murchison. *An evaluation of py relationships in sands*. University of Houston, 1983.

[24] Ian Prowell. *An experimental and numerical study of wind turbine seismic behavior*. PhD thesis, UC San Diego, 2011.

[25] Lymon C Reese, William R Cox, and Francis D Koop. Analysis of laterally loaded piles in sand. *Offshore Technology in Civil Engineering Hall of Fame Papers from the Early Years*, pages 95–105, 1974.

[26] Marc Seidel, Sven Voormeeren, and Jan-Bart van der Steen. State-of-the-art design processes for offshore wind turbine support structures: Practical approaches and pitfalls during different stages in the design process. *Stahlbau*, 85(9):583–590, 2016.

[27] Peter M Shearer. *Introduction to seismology*. Cambridge university press, 2019.

[28] V Valamanesh and AT Myers. Aerodynamic damping and seismic response of horizontal axis wind turbine towers. *Journal of Structural Engineering*, 140(11):04014090, 2014.

[29] Norske Veritas. *Guidelines for design of wind turbines*. Det Norske Veritas: Wind Energy Department, Ris National Laboratory, 2002.

[30] WG Versteijlen, FW Renting, PLC Van Der Valk, J Bongers, KN Van Dalen, and AV Metrikine. Effective soil-stiffness validation: Shaker excitation of an in-situ monopile foundation. *Soil Dynamics and Earthquake Engineering*, 102:241–262, 2017.

[31] WG Versteijlen, JM de Oliveira Barbosa, KN van Dalen, and AV Metrikine. Dynamic soil stiffness for foundation piles: Capturing 3d continuum effects in an effective, non-local 1d model. *International Journal of Solids and Structures*, 134:272–282, 2018.

[32] ACWM Vrouwenvelder. *Random Vibrations: CT5145*. TU Delft, 2004.

[33] E Winkler. Die lehre von elastizitat und festigkeit (on elasticity and fixity). *Dominicus, Prague*, 1867.

[34] David Witcher. Seismic analysis of wind turbines in the time domain. *Wind Energy: An International Journal for Progress and Applications in Wind Power Conversion Technology*, 8(1):81–91, 2005.

[35] John P Wolf. Soil-structure interaction. *Prentice Hall Inc., Englewood Cliffs, New Jersey ISBN 0 l3*, 221565 (9):01, 1985.

[36] X Zhao and P Maisser. Seismic response analysis of wind turbine towers including soil-structure interaction. *Proceedings of the Institution of Mechanical Engineers, Part K: Journal of Multi-body Dynamics*, 220(1):53–61, 2006.

[37] Olek C Zienkiewicz and Robert L Taylor. *The finite element method for solid and structural mechanics*. Elsevier, 2005.